Core–shell polymeric nanoparticles comprising BODIPY and fluorescein as ultra-bright ratiometric fluorescent pH sensors

Chloé Grazon, Yang Si, Jean-Pierre Placial, Jutta Rieger, Rachel Méallet-Renault, Gilles Clavier

Core-shell polymeric nanoparticles comprising BODIPY and fluorescein as ultra-bright ratiometric fluorescent pH sensors

C. Grazon,*[,a,†] Y. Si,[a] J.-P. Placial,[a] J. Rieger,[b] R. Méallet-Renault[a,§] and G. Clavier[a]

[a] PPSM, ENS Cachan, CNRS, Université Paris-Saclay, 94235 Cachan, France. E-mail: chloe.grazon@u-bordeaux.fr.

[b] Sorbonne Université, CNRS, Institut Parisien de Chimie Moléculaire, UMR 8232, Team : Chimie des Polymères, 75005 Paris, France.

Current addresses: † Laboratoire de Chimie des Polymères Organiques (LCPO), CNRS UMR 5629, Université de Bordeaux, Bordeaux-INP, Pessac 33607 Cedex, France §Institut des Sciences Moléculaires d'Orsay (ISMO), CNRS, Univ. Paris-Sud, Université Paris-Saclay, F-91405 Orsay (France).

Summary

A new ratiometric fluorescent pH nanosensor is presented. It is based on ultrabright nanoparticles containing two spatially separated fluorophores: BODIPY covalently linked to the polystyrene core and fluorescein grafted to the nanoparticle shell. The nanoparticles comprise a large number (≥2500) of both fluorescent moieties. Their spectroscopic characteristics were studied at different pH and ionic strength. They could successfully be used to determine the solution pH between 5.5 and 7.5 by measuring the fluorescence intensity ratio of the sensor molecule (fluorescein) relative to the reference dye (BODIPY).

Introduction

Optical imaging is becoming increasingly attractive in medicine, biology and biochemistry since it can achieve high spatial and temporal resolution and is non-invasive. Many optochemical sensors have been developed to detect analytes, such as metal ions, oxygen, reactive oxygen species, or to determine physico-chemical parameters such as pH, temperature or viscosity, both *in vitro* and *in vivo*.[1, 2] One of the most relevant parameters to be monitored is the pH, since it is highly regulated in the body. For instance, small variations of pH can affect protein activity.[3] Diseases can induce variations of pH leading to modified functionality of tissues or cells. Cancer cells and healthy cells can be distinguished by their proton activity, the former being more acidic than the latter.[4]

Fluorescence is a very sensitive technique amenable to miniaturization, high sensitivity and cost effectiveness. Hence, many organic fluorescent molecules modified to sense a particular analyte or parameter have been reported.[5, 6] Among them, pH-sensitive fluorophores such as seminaphthorhodafluors or seminaphthofluoresceins have been widely used to measure pH in cells.[7] However, organic molecules have many limitations in such applications. Their most common shortcomings are dye aggregation in water or accumulation in specific cell compartments, loss of photophysical properties in polar media and toxicity. Fluorescent nanoparticles have thus been developed recently in order to circumvent these restrictions while maintaining the interesting properties of organic dyes. In particular, this approach allows fluorophore loading inside a particle which limits its toxicity. It is also possible to post-functionalize the particles surface/shell in order to enhance biocompatibility, cell permeability and permit specific targeting.[8] Various approaches have been developed to this end.[9] One of

the most popular to date is the use of quantum dots. These nanoobjects have the advantage of being intrinsically luminescent, small (a few nanometers) and their color is easily tuned by modifying the size. Their surface can be decorated with functional ligands possessing, for example, sensing abilities.[10] However, serious questions remain concerning their toxicity since they are made of noxious heavy metals and also their lack of stability, especially in dilute complex media like cells.[11] Silica nanoparticles, to which multiple fluorophores and sensing units can be covalently grafted, are also very promising materials.[12, 13] Their size is tunable from 10 nm to a few hundreds of nm and they have emerged as a promising class of nanomaterial for bioimaging and sensing. Nevertheless, water-sensitive fluorophores might not be compatible with this approach and the question of their toxicity remains disputed (see ref. [13] for a discussion). Moreover, those nanoparticles also suffer from stability in water due to the slow dissolution of silica over time.

Finally, nanoparticles based on assemblies of organic polymers are especially attractive since they offer a great variability of monomer structures and synthetic pathways making them compatible with most common organic fluorophores.[14] They also permit easy integration of two or more fluorophores to achieve ratiometric detection.[15] The main advantage of the ratiometric approach is that changes in the fluorescence signal caused by a variation of concentration of the sensor or by light fluctuation are internally corrected by the measurement of two signals.

There are various examples of pH-sensitive fluorescent and ratiometric polymeric nanoparticles (FNP) reported to date, which vary in polymer nature, particle size, nature of the fluorophore... They can be classified in two groups: for the first one, a fluorescence intensity ratio of a pH-sensitive probe and a pH-insensitive reference fluorophore (used as an internal reference) is determined;[16-21] for the second class, both dyes are sensitive to the analyte but reacts in opposite direction; thus the signal ratio originates from two inversely varying bands.[22-24] Polymer-based fluorescent nano-objects can have very different compositions and structures, such as micelles (i), hydrogels nanoparticles (NP) (ii) or nano-sized particles (iii). For instance, Shiyong Liu *et al*.[14, 22] synthesized - by RAFT copolymerization – pH-sensitive fluorescent micelles (i) composed of thermosensitive amphiphilic block copolymers comprising three different dyes (pH-sensitive Rhodamine B, photoswitchable spyropyran and a reference). The fluorescence emission of the micelles changed with temperature, pH or exposition to UV. The authors succeeded to measure the pH from 3 to 6. Andresen *et al.* studied hydrogel-based FNP (ii), functionalized by two different pH sensitive dyes (a fluorescein derivative and Oregon green) and a reference dye (Alexa 633).[16] Using such a complex system comprising two pH-sensitive dyes allowed them to sense pH from 3.9 to 7.9, which is useful for intracellular studies of endosomes or lysosomes.[17] Finally, nanostructured FNP (iii) have also been studied, for instance by Zhang *et al.*[25, 26] Using miniemulsion polymerization, they immobilized a naphtalimide derivative in the hydrophobic core of the FNP and post-functionalized the hydrophilic surface with a fluorescein derivative. Using this strategy, up to 3375 dyes per FNP could be inserted. By recording a fluorescence signal due to FRET from the naphtalimide to the fluorescein, they were able to determine pH values between 3 and 8.

However, in most of those examples of polymeric FNP, no full characterization of the fluorescence is reported. Most importantly, the number of fluorophores and the fluorescence quantum yields (Φ_F) are rarely determined. This is a major drawback since, in the frame of bioimaging, high brightness ($B = \varepsilon \times \Phi_F$) is of utmost importance to guarantee that a good fluorescence signal will be detected at low NP loading.[27]

We have recently developed a novel, straightforward synthesis strategy to prepare fluorescent, nanostructured (core-shell) polymeric nanoparticles (Schemes S1 and S2).[28, 29] They were constituted of a hydrophilic shell made of either a poly(ethylene oxide)-*b*-poly(acrylic acid) (PEO-*b*-PAA) *diblock* copolymer (Scheme S1) or a *randomly* distributed copolymer of acrylic acid (AA) and poly(ethylene oxide) methyl ether acrylate (PEOA) (Scheme S2). The shell was covalently linked to a hydrophobic core, a copolymer of styrene and a BODIPY (BOD) monomer. They were prepared in a simple miniemulsion polymerization one-pot process, which uses neither ultra-hydrophobic agents, nor low molar mass surfactants - which may be detrimental to the targeted biological applications. Most importantly, these FNP comprise a large number of fluorophores in their core (> 1900) and reactive carboxylic acid functions in their shell. These nanoparticles have been shown to be extremely brilliant (brightness in the order of 10^7 $M^{-1}.cm^{-1}$).

In this work, we report their modification to develop ultrabright pH-sensitive fluorescent nanoparticles. Fluorescein has been chosen since it is a highly fluorescent pH-sensitive probe.[30] A large variety of fluorescein derivatives have been formerly studied, such as fluorescein isothiocyanate, or alkyne-derived fluorescein, which can be attached to polymer chains. In our approach, we choose to functionalize the poly(acrylic acid)-based shell of our nanoparticles with fluoresceinamine (FA) through an amide coupling.[31] BODIPY and fluorescein have already been combined to realize a molecular ratiometric FRET sensor for cysteine,[32] but to the best of our knowledge, this is the first time that BODIPY and fluorescein are covalently immobilized in polymeric nanoparticles to elaborate nano-sized pH nanosensors.

Materials and methods

NMR: ^{1}H NMR spectra were recorded in $CDCl_3$ on a JEOL ECS (400 MHz) spectrometer. All chemical shifts were referenced to Me_4Si. In order to monitor the individual molar conversion of acrylic acid (AA) and PEOA, DMF (7.95 ppm) was used as internal standard and conversions were determined by the relative decrease of the acrylate signals between 6.4 and 5.8 ppm to DMF.

pH measurement was performed using a glass electrode connected to a PHM210 Standard pH meter from Meterlab.

SEC: the number-average molar mass (M_n), the weight-average molar mass (M_w), and the molar mass distribution (molar massdispersity M_w/M_n) were determined by size exclusion chromatography (SEC) using THF as an eluent at a flow rate of 1 $mL.min^{-1}$. For analytical purposes, the acidic functions of the block or alternated copolymers were turned into methyl esters.[33] Therefore, the copolymers were recovered by drying of the aqueous suspensions. After dissolution in a THF/H_2O mixture and acidification of the medium with a 1M HCl solution, they were methylated using an excess of trimethylsilyldiazomethane. Polymers were analyzed at a concentration of 5 $mg.mL^{-1}$ in THF after filtration through 0.45 µm pore size membrane. The SEC apparatus was equipped with a Viskotek VE 2100 automatic injector and two columns thermostated at 40°C (PLgel Mixed, 7.5 mm × 300 mm, bead diameter: 5 µm). Detection was made with a differential refractive index detector (Viscotek VE 3580 RI detector) and a UV-vis. detector (Waters 486 Tunable Absorbance Detector). The Viscotek OmniSEC software (v 4.6.2) was used for data analysis and the relative M_n and M_w/M_n were calculated with a calibration curve based on polystyrene standards (from Polymer Laboratories).

Quantitative Elementary microanalyses of Oxygen, Nitrogen and Sulfur were performed at the Institut de Chimie des Substances Naturelles of Gif-sur-Yvette (France) service in order to determine the grafting efficiency of ethanolamine (EtA). The polymer nanoparticles were purified by dialysis (MWCO: 300 kDa, Spectrapor) for 7 days in MQ water in the dark and then lyophilized. Each sample has been analyzed three times and values are given with an error of ± 0.30%.

The z-average hydrodynamic particle diameter (named D_h) and the particle size distribution (dispersity factor, named σ), were determined by dynamic light scattering (DLS) of the diluted aqueous dispersions at 20°C, at an angle of 90°, with a Zetasizer Nano S90 from Malvern, using a 4 mW He-Ne laser at 633 nm. A dispersity factor (σ) below 0.1 is characteristic of a narrow particle size distribution. All calculations were performed using the Nano DTS software.

Zeta potentials (ζ) were performed on a Zetasizer Nanoseries (Malvern) apparatus at the Institut Curie, Paris, France. Samples were prepared at concentration of 0.005 wt% diluted in 14mM NaCl water, buffered with 1mM of phosphate/citrate salts (pH values varied from 4 to 8). Samples were analyzed in DTS 1060 plastic cells, at 25°C. Three measures of ten scans were performed for each sample. The value is the average of those 30 measurements, and the standard deviation is between 5 and 10% of the value depending on the samples.

TEM: conventional transmission electron microscopy was performed on a JEOL JEM CX II UHR microscope operating at 100 keV and equipped with a Keen View CCD camera from Soft Imaging System (Olympus) calibrated with three polystyrene particle samples (PELCO 610-SET - 91, 300, and 482 nm, Ted Pella Inc.). The acquisition was done with the iTEM software from Soft Imaging System (Olympus). The samples were diluted in water prior to analysis and then deposited on a carbon-coated copper grid.

UV-visible spectra were recorded on a Varian Cary (Palo Alto, CA USA) double beam spectrometer using a 10 mm path quartz cell from Thuet (Bodelsheim, France). Excitation and emission spectra were measured on a SPEX Fluoromax-3 (Horiba Jobin-Yvon). A right-angle configuration was used. Optical density of the samples was checked to be less than 0.1 to avoid reabsorption artifacts. Fluorescence quantum yields Φ_F were determined using sulforhodamine 101 (Φ_F = 0.9 in ethanol)[34] as a reference and are given with a 5% instrument error.

Fluorescence decay curves were obtained with a time-correlated single-photon-counting method using a titanium-sapphire laser (82 MHz, repetition rate lowered to 4 MHz thanks to a pulse-peaker, 1 ps pulse width, a doubling crystals is used to reach 495 nm excitation) pumped by an argon ion laser from Spectra Physics (Mountain View, CA USA).

Average fluorescence lifetimes were calculated by global integration of the decays using the equation:[35]

$$<\tau>=\frac{\int_0^\infty tI(t)dt}{\int_0^\infty I(t)dt} \quad (1)$$

where *I(t)* is the fluorescence intensity at time *t* of the decay. Average lifetime are given with 1% error due to the instrument and fit analysis.

Materials

Fluoresceinamine, isomer I (Aldrich, FA), 1-ethyl-3-(3-dimethylaminopropyl) carbodiimide hydrochloride (Fluka, > 98%, EDC), ethanolamine (Sigma-Aldrich, >99%, EtA), acrylic acid (Aldrich, 99%, AA), poly(ethylene oxide) methyl ether acrylate (Aldrich, M_n=480 g/mol, PEOA), citric acid (Carlo Erba, 99.8%), sodium phosphate dibasic dihydrate (Sigma-Aldrich, > 99.5%), 2-methyl-2-[(dodecylsulfanylthiocarbonyl)sulfanyl] propanoic acid (Strem, > 97%, TTC) were used as received. Styrene was distilled under reduced pressure. BODIPY monomer (2,6-diethyl-4,4-difluoro-8-(4-(methacryloyloxy)-phenyl)-1,3,5,7-tetramethyl-4-bora-3a,4a-diaza-s-indacene, BOD) was synthesized as reported.[28] Solvents were purchased from Carlo Erba. Deionized water (15MΩ.cm at 20°C) was prepared with a Milli-Q system (Millipore).

Synthesis of macroRAFT agents

PEO_{45}-*b*-PAA_y-TTC (y = 15 or 19) diblock copolymer macroRAFT agents were synthesized as described elsewhere (PEO_{45}-*b*-PAA_{15}-TTC $M_{n\ NMR}$ = 3.5 kg/mol, $M_{n\ SEC}$ = 4.3 kg/mol, M_w/M_n = 1.06; PEO-*b*-PAA_{19}-TTC $M_{n\ NMR}$ = 3.8 kg/mol, $M_{n\ SEC}$ = 3.9 kg/mol, M_w/M_n = 1.09, PS calibration).[28] The synthesis of the P($PEOA_{0.5}$-co-$AA_{0.5}$)$_{22}$-TTC random copolymer macroRAFT agent has also been described previously ($M_{n\ NMR}$ = 6.2 kg/mol, $M_{n\ SEC}$ = 6.0 kg/mol, M_w/M_n = 1.16, PS calibration).[36, 37]

Synthesis of fluorescent nanoparticles

The copolymerization of styrene and BODIPY monomer (BOD) was performed in the presence of a macro-RAFT agent functionalized by a trithiocarbonate function, PEO-*b*-PAA-TTC[28] (FNP1) or P($PEOA_{0.5}$-*co*-$AA_{0.5}$)$_{22}$-TTC[37] (FNP2) in a one-pot miniemulsion phase inversion process as described before.

Functionalization of nanoparticles with fluoresceinamine

In a typical experiment, 0.3 mL of a pristine nanoparticle batch (0.1 mg/mL) was diluted in 4 mL of water in the dark. In parallel, 0.5 (**$FNP1_{BOD}$**) or 1 (**$FNP2_{BOD}$**) equivalents of FA (3.35 or 6.7 mg) compared to the acrylic acid units was dissolved in 0.4 mL of ethanol. Once the FA was dissolved, the solution was added to the nanoparticles solution and the mixture was vigorously stirred at 4°C. Then, a solution of EDC (4 equiv., 15 mg) in water (1 mL) was added to the previous mixture. To quench the reaction, ethanolamine (2 equiv., 2.3 µL) was added 2 hours later. The reaction solution was still stirred at 4°C for 12h in the dark. Finally, the mixture was transferred in a cellulose ester dialysis membrane (MWCO: 300 kDa, Spectrapor) and dialyzed against ultra-pure water for 7 days in the dark.

Results and discussion

Synthesis of FNP

The ratiometric pH nanosensors were prepared using reactive polymeric fluorescent nanoparticles (FNP), whose synthesis has been reported recently.[28, 37] As mentioned above, it consists of a one-pot synthesis based on a reversible addition−fragmentation chain-transfer (RAFT) polymerization in

miniemulsion conditions.[38, 39] Two types of macro-RAFT agents with different architectures were used to prepare the core-shell nanoparticles. The first one was a hydrophilic *diblock* copolymer prepared from a polyethylene oxide (PEO) chain (M_n = 2 kg/mol) end-functionalized with a trithiocarbonate (TTC) RAFT agent, which was block-extended with 15 or 19 units of acrylic acid (AA) providing a double hydrophilic macromolecular RAFT (macroRAFT) agent, PEO-*b*-PAA-TTC, equally end-capped by a trithiocarbonate function (Scheme S1). The second one was a *randomly* distributed copolymer of acrylic acid (AA) and poly(ethylene oxide) methyl ether acrylate (PEOA, average M_n = 480 g/mol), which were copolymerized in the presence of the TTCA RAFT agent (Scheme S2). The hydrophilic macroRAFT agents were then used in the copolymerization of styrene (S) with the polymerizable BODIPY fluorophore (BOD) in a one-pot miniemulsion phase inversion process as described before.[28, 37]

Table 1 Composition and characterization of FNP in water (pH=8)

Sample	Core composition	Shell composition	Grafted molecule	N_{agg}[a]	N_{BOD}[b]	N_{FA}[b]	D_h/nm (σ)[c]
FNP1$_{BOD}$	S-*co*-BOD	PEO_{45}-*b*-PAA_{15}	-	1750	1930	-	76 (0.12)
FNP1$_{FA}$*	S	PEO_{45}-*b*-PAA_{19}	FA + EtA	1750	-	530	73 (0.23)
FNP1$_{BOD-FA}$	S-*co*-BOD	PEO_{45}-*b*-PAA_{15}	FA + EtA	1750	1930	1140	68 (0.10)
FNP2$_{BOD}$	S-*co*-BOD	$P(PEOA_{0.5}$-*co*-$AA_{0.5})_{22}$	-	1030	1960	-	77 (0.10)
FNP2$_{FA}$*	S	$P(PEOA_{0.5}$-*co*-$AA_{0.5})_{22}$	FA + EtA	1030	-	340	56 (0.06)
FNP2$_{BOD-FA}$	S-*co*-BOD	$P(PEOA_{0.5}$-*co*-$AA_{0.5})_{22}$	FA + EtA	1030	1960	540	68 (0.14)

[a] Nanoparticle aggregation number (equation S1), given with 15% error. [b] Respectively number of BODIPY monomer (equation S3) and FA per nanoparticle. [c] Hydrodynamic diameter and dispersity factor given in brackets. * Already published data [40]

Fluorescent nanoparticles, in which BODIPY is covalently linked to the polymer chains, **FNP1$_{BOD}$** and **FNP2$_{BOD}$**, were obtained. The FNP were well-defined in size as shown by DLS measurements (mean hydrodynamic diameter: 76 and 77 nm respectively; (σ: 0.12 and 0.10 respectively, Table S1). The number of BODIPY per particle could be calculated using equation S3 and was close to 2000 in both cases (Table 1). Both types of FNP synthesized have carboxylic acid groups in the shell allowing a post-functionalization with amine molecules and the preparation of ratiometric nanosensors.

BODIPY-free non-fluorescent nanoparticles, but otherwise similar in composition to **FNP1$_{BOD}$** and **FNP2$_{BOD}$**, were also prepared using the same protocol and used as reference nanoparticles **FNP1** and **FNP2** in Table S1). Fluoresceinamine has already successfully been grafted on this blank nanoparticles and their sensitivity to pH measurement demonstrated,[40] providing thus good reference samples.

Grafting on the FNP

Grafting of amine-functionalized molecules on carboxylic groups is a standard procedure.[41] It is usually performed using an activated ester. One of the most common protocols for ester activation uses EDC and *N*-hydroxysuccinimide (NHS). However, this protocol is very sensitive to reaction conditions (temperature and pH). It was tested on **FNP1$_{BOD}$** at pH=7 at room temperature, but irreversible precipitation of the

nanoparticles occurred and the reaction did not take place. Substitution of NHS by hydroxybenzotriazole gave the same results. It has already been shown that using EDC alone in excess (at least two folds) is sufficient to perform grafting of PAA on the terminal amine functions of nylon 6,6.[42] However, the activated ester was quickly hydrolyzed at pH>7 at room temperature. On the other hand, amines react faster when they are non-protonated, *i.e*. in alkaline conditions. Furthermore, **FNP1$_{BOD}$** precipitate at pH<6.[28] These seemingly contradictory conditions could be overcome when working at low temperatures at which the activated ester is more stable. Hence the functionalization of the FNP with an amine containing molecule was carried out at pH=8 and 4 °C using a 4-fold excess of EDC per carboxylic acid.

The grafting efficiency was first tested using ethanolamine (EtA) as a model primary amine. Three equivalents of the amine per acrylic acid were used. The percentage of grafted amines was determined by microanalysis and comparison of the weight percentage of nitrogen and oxygen. The degree of grafting on **FNP1$_{BOD}$** and **FNP2$_{BOD}$** was 62 (±4)% and 56 (±3)% respectively. In both cases, the hydrodynamic diameter of the FNP was unchanged after reaction with ethanolamine. It has formerly been shown that ungrafted FNP precipitated at pH below 5, probably due to the formation of hydrophobic complexes between ethylene oxide and acrylic acid at acidic pH.[43] Contrariwise, the FNP derivatised with ethanolamine were stable at all investigated pH (from 4 to 8) and did not precipitate in acidic media. This increased stability was another proof for successful grafting. Particle stability over a broader range of pH is actually crucial for the targeted sensing applications. Those optimized reaction conditions were then used to graft fluoresceinamine (FA) on the acrylic acid shell of the nanoparticles.

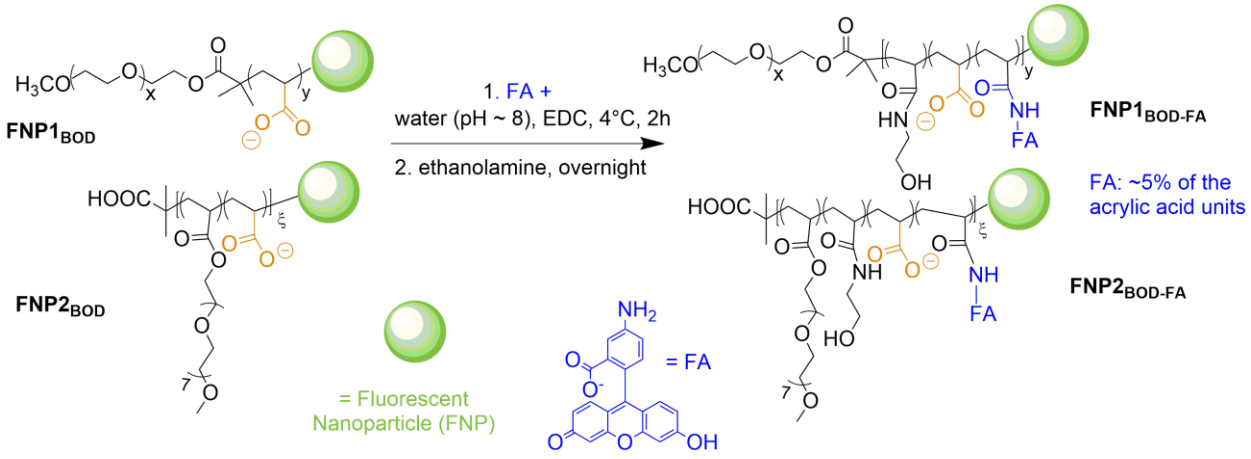

Scheme 1 Preparation of pH nanosensors from **FNP1$_{BOD}$** and **FNP2 $_{BOD}$** (green spheres schematize the hydrophobic P(S-*co*-BOD) core of the FNP, FA stands for fluoresceinamine).

Fluorescein was selected as a pH-sensitive molecule because it has an intense absorption in the visible. Even though it can adopt four different forms (dianion, anion, neutral and cation) depending on the pH, it is only highly fluorescent in its dianionic form.[30] Furthermore the pK_a of the anion/dianion couple is about 6.4, which is convenient to sense pH in biological media. The grafting of FA on **FNP1$_{BOD}$** and **FNP2$_{BOD}$** was carried out (Scheme 1) using 0.5 and 1 equivalents of FA per acrylic acid unit respectively. After 2 hours of reaction, ethanolamine was added to react with the remaining carboxylic acid groups in order to ensure colloidal stability of the FNP in acidic media. As control, FA was grafted on blank nanoparticles which did not contain BODIPY. These nanoparticles, **FNP1$_{FA}$** and **FNP2$_{FA}$,** were used as references. In all cases, the grafting did not significantly change the hydrodynamic diameter of the nanoparticles (Table 1) and particle integrity was maintained as shown by TEM (Figure S1).

The zeta potentials (ζ) of the FNP were then determined at different pH values (Table 2). The macromolecular architecture of the hydrophilic block played an important role since large differences could be noted for **FNP1$_{BOD}$** and **FNP2$_{BOD}$**. In the first case (**FNP1$_{BOD}$**), between pH 6 and 8 the FNP possess an apparent negative ζ-potential. The negative value is in accordance with values reported for pegylated polystyrene particles without PAA.[43]

It seemed that the outermost PEO block screens the charges of the PAA middle block – as the protonation of acrylic acid units was not detected.[44] This result was confirmed with **FNP1$_{BOD-EtA}$**. In these nanoparticles, 60% of the acrylic acids were derivatised with ethanolamine but the apparent charge remained unchanged. The same situation was found for fluorescein-grafted nanoparticles, **FNP1$_{FA}$** and **FNP1$_{BOD-FA}$**. The only difference was that all grafted **FNP1** remained stable at pH<5 while **FNP1$_{BOD}$** precipitated. On the contrary, the ζ-potential of **FNP2$_{BOD}$**, possessing a random copolymer of AA and PEOA as shell, decreased with decreasing pH. In this case the acrylic acids seem more exposed to the external media, and their protonation led to a measurable decrease of the zeta potential. After reaction with amines, those FNP had a lower apparent charge in alkaline media (see **FNP2$_{FA}$** and **FNP2$_{BOD-FA}$**), which also decreased at lower pH values. In contrast to the **FNP1** series, all **FNP2** particles were stable at all pH investigated (from 4 to 8) revealing the impact of the architecture of the stabilizing polymer (double hydrophilic block copolymer *vs*. random graft copolymer) on the pH stability.

Hence, the measurement of zeta potentials at various pH revealed that the grafting reaction was effective on both types of FNP and made them stable at all pH.

Table 2 Zeta potentials in mV recorded in water at RT in saline water ([NaCl]= 14 mM) for different pH values (phosphate-citrate buffers 1mM).

Sample	pH = 4	pH = 6	pH = 7	pH = 8
FNP1$_{BOD}$	[a]	-17	-14	-16
FNP1$_{FA}$	-9	-14	-	-14
FNP1$_{BOD-FA}$	-11	-	-15	-15
FNP1$_{BOD-EtA}$	-16	-14	-12	-15
FNP2$_{BOD}$	-16	-29	-36	-30
FNP2$_{FA}$	-1	-18	-	-21
FNP2$_{BOD-FA}$	+5	-12	-16	-21

[a] **FNP1$_{BOD}$** precipitate at pH 4.

Spectroscopic properties of the FNP

First of all, the nanoparticles containing only BODIPY were studied in various media. Their absorption and emission spectra are shown in Figure 1 and Figure S2, their fluorescence decays in Figure S15 and their main spectroscopic data are given in Table 3.

The spectroscopic features of **FNP1$_{BOD}$** and **FNP2$_{BOD}$** were similar (same absorption and emission maxima and average fluorescence lifetime) at the exception of the fluorescence quantum yield which was 1.5 higher in the second case. This may be related to the change in the local environment of the dye.[37] For both types of FNP, the number of BOD/particle was large (1930 and 1960) and the fluorescence quantum yields were high (39% and 56% for **FNP1$_{BOD}$** and **FNP2$_{BOD}$** respectively). As a consequence, the brightness (*B,* equation S4) of these nanoparticles was very high (approx. 2×10^7 $M^{-1}.cm^{-1}$).[29]

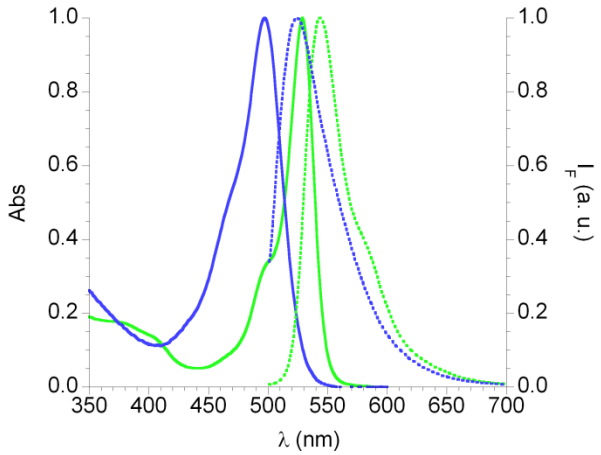

Fig. 1 Normalized absorption (full lines) and fluorescence emission spectra (dotted lines, λ_{exc} = 495 nm) of **FNP2$_{BOD}$** (green) and **FNP2$_{FA}$** (blue) at pH = 8

Fluorescence emission and excitation spectra of both types of FNP have been recorded at various pH (from 5 to 8) using a total concentration of phosphate/citrate buffers of 1 or 10 mM and 140 mM NaCl (figures S3-6). In all cases neither spectral variation nor major intensity changes were observed (relative variations lower than 5%). The effect of salt concentration was also studied (figures S7 and S8). The NaCl concentration was varied from 14 to 140 mM and fluorescence emission spectra recorded at three pH (4.7, 5.7 and 7.2) without any alteration of shape or intensity. In conclusion, pH and ionic strength variations have no influence on the BODIPY fluorescence in the FNP.

The grafting of ethanolamine did not alter the position and shape of the absorption and emission spectra of the BODIPY (see **FNP1$_{BOD\text{-}EtA}$** in Table 3) but the fluorescence quantum yield was decreased. Incubating **FNP1$_{BOD}$** with EDC alone gave the same result. Thus the grafting conditions decreased the fluorescence quantum yield of BOD in the FNP. However, the large number of fluorophores in the nanoparticles ensured that they were still very bright ($B > 1\times10^7$ $M^{-1}.mol^{-1}$).

The spectroscopic properties of BODIPY-free nanoparticles grafted with fluoresceinamine (FA), **FNP$_{FA}$**, have already been studied[40] and are recalled in Table 3 and in Figure 1 (pH=8), S9 and S10. They were shown to respond to pH variation similarly to fluorescein dissolved in water (Figures S9 and S10). The calculated pK_a for both types of FNP was 6.55±0.02.[40] The number of grafted FA was 530 and 340 for **FNP1$_{FA}$** and **FNP2$_{FA}$** respectively (Table 1).

In order to obtain ratiometric pH-sensitive nanoparticles, FA has been grafted on the BODIPY containing nanoparticles. Within the absorption spectra of **FNP1$_{BOD\text{-}FA}$** and **FNP2$_{BOD\text{-}FA}$** two main bands in the visible region are present at 495 and 528 nm. Their respective intensities vary with the pH and correspond to

fluorescein and BODIPY respectively (Figures S11 and S12). The number of FA compared to BODIPY could be estimated from the absorption spectra at pH=8, using $\varepsilon_{BOD}(528)=73000\ M^{-1}.cm^{-1}$ and $\varepsilon_{FA}(495)=88000\ M^{-1}.cm^{-1}$ [45]. For **FNP1$_{BOD-FA}$** a number of 0.58 FA per BODIPY molecules and for **FNP2$_{BOD-FA}$** 0.28 FA per BODIPY were calculated. Since the number of BODIPY per nanoparticle had been determined, it was possible to estimate the number of grafted FA per polymer chain and thus the grafting efficiency. For **FNP1$_{BOD-FA}$** 4% of the AA units had been successfully grafted (0.5 eq FA/AA introduced, grafting efficiency 8%) and for **FNP2$_{BOD-FA}$** 5% of the AA units had been functionalized (1 eq FA/AA introduced, grafting efficiency 5%). It seemed that it was easier to graft a dye on the block copolymer PEO_{45}-*b*-PAA_{15} or PAA_{19} than on the random copolymer $P(PEOA_{0.5}$-*co*-$AA_{0.5})_{22}$. This could be related to steric hindrance resulting from the dense PEO grafts separated by only one AA unit on average (equimolar composition in AA and PEOA). However, in all cases the reaction yields were higher than the one reported by Déjugnat *et al.* who could only graft 0.7% of the AA units with FA in DMF/water 5/95 with EDC.[46] The fluorescence spectra at pH=8 of **FNP1$_{BOD-FA}$** (Figure 2 left) and **FNP2$_{BOD-FA}$** (Figure S12 top right) showed a main band centered at 544 nm and a less intense shoulder at higher energy (around 515 nm). The main band was attributed to BODIPY and the shoulder to the grafted FA. It is important to note that both bands could be observed under a single excitation wavelength chosen at 495 nm where both fluorophores absorb light. The fluorescence spectra were then recorded at different pH (phosphate/citrate buffers 10 mM in 140 mM NaCl). Both the intensity of BODIPY and FA increased with pH for both types of nanoparticles. Since it was demonstrated on **FNP$_{BOD}$** that the pH has no influence on the BODIPY emission, the increase in the region of the BODIPY emission was likely due to an overlap with the fluorescence band of the FA dianion which extended to 600 nm.[30]

Table 3 Spectroscopic data of FNP in water (pH=8)

Sample	λ_{abs} / nm	λ_{em}[a] / nm	Φ_F [b]	$<\tau_{515}>$[c] / ns	$<\tau_{543}>$[c] / ns	$B\times10^{-7}$ [d] / $M^{-1}\ cm^{-1}$
BOD*	528	540	0.69		4.9	1.7×10^{-3}
FNP1$_{BOD}$	529	544	0.39		4.3	1.9
FNP1$_{FA}$	494	522	0.12	2.2	2.2	0.6
FNP1$_{BOD-FA}$	495; 528	544	0.08	3.1	1.6	1.2
FNP1$_{BOD-EtA}$	529	544	0.26			1.3
FNP2$_{BOD}$	529	544	0.52		4.5	2.5
FNP2$_{FA}$	497	524	0.14	2.7	2.6	0.4
FNP2$_{BOD-FA}$	495; 528	544	0.12	2.6	1.6	1.2

[a] λ_{ex} = 495nm. [b] Fluorescence quantum yield, reference sulforhodamine 101 (Φ_F = 0.9 in ethanol).[34] [c] Average lifetime according to equation 1 (λ_{exc} = 495 nm) at respectively λ_F = 515 nm and λ_F = 543 nm. [d] Fluorescence Brightness when samples are excited at 495 nm, calculated using equation S4 for $FNP1_{BOD}$, $FNP1_{FA}$, $FNP1_{BOD-EtA}$, $FNP2_{BOD}$, $FNP2_{FA}$ and equation 3 for $FNP1_{BOD-FA}$ and $FNP2_{BOD-FA}$. *Spectroscopic properties of BOD in toluene.

However, at this point we cannot exclude the occurrence of resonant energy transfer (RET) from FA (emission 522nm) to BODIPY (absorption 528nm). Indeed, the Förster radius of the grafted FA (donor) in its dianionic form (Φ_F = 13±1%) and the BOD (acceptor) inside the NPF is estimated as 4.1±0.1 nm (using an orientation factor κ = 0.457); while the end-to-end distance of a poly(acrylic acid) chain of 15 units at pH > 7 is approximately 4.8 nm (calculated using the Flory characteristic ratio). As such, it is in theory possible that FRET occurs from FA to BOD.

In order to measure RET, we first recorded excitation spectra of **FNP1$_{FA}$** and **FNP1$_{BOD\text{-}FA}$** at four different pH (from 4 to 8) and at three different emission wavelength (λ_F = 515, 542 and 587 nm) (Figures S13 and S14). Unfortunately, due to spectral overlap of the fluorescence emission of BOD and FA, we were not able to selectively excite FA only and record energy transfer to BOD.

Hence fluorescence decays of **FNP1$_{BOD\text{-}FA}$** and **FNP2$_{BOD\text{-}FA}$** were recorded in water at pH=7.8 and compared to those of the corresponding nanoparticles containing only either BODIPY or FA (Figure S7). Indeed, the RET phenomenon has a strong impact on the fluorescence lifetime of the donor which is shortened in the presence of the acceptor. Furthermore, the decay of the acceptor should also contain a rising time proportional to the transfer rate which can however be hard to detect if it is too short for the set up used.[35]

In both cases, the excitation wavelength was set at 495 nm and decays of nanoparticles containing fluorescein were recorded at 515 and 543 nm (Figure S15). The decays were multiexponential and only average lifetimes were extracted by global analysis (see materials and methods for details). The average fluorescence lifetimes (Table 3) of FA in **FNP1$_{FA}$** were similar at both wavelengths (2.2 ns). The same result was observed for **FNP2$_{FA}$** ($<\tau>$=2.6 and 2.7 ns at 515 and 543 nm respectively). FA was the only emitting species in both FNP. The average fluorescence lifetimes of **FNP1$_{BOD\text{-}FA}$** and **FNP2$_{BOD\text{-}FA}$** at 515 nm (where only FA emits) were 3.1 and 2.6 ns respectively. It is difficult to understand why, in the case of **FNP1$_{BOD\text{-}FA}$,** there was an increase in the fluorescence lifetime. Nevertheless, there was no shortening of the lifetimes of the donor (FA) which would be a sign of energy transfer to the BODIPY. The fluorescence lifetimes at 543 nm (where BODIPY emission was predominant) of both **FNP1$_{BOD\text{-}FA}$** and **FNP2$_{BOD\text{-}FA}$** were shorter than those of **FNP1$_{BOD}$** and **FNP2$_{BOD}$**. This was in line with the observed loss of fluorescence quantum yield of the BODIPY upon grafting FA on the nanoparticles. Inspection of the early part of the decays of both nanoparticles at 543 nm did not let appear a rising time. These results let us conclude that there was no detectable energy transfer from FA to BODIPY in the grafted nanoparticles. Hence the BODIPY could be considered as the reference fluorophore and the FA as the sensing one.

Further insight in the spectral evolution with pH was gained from a mathematical analysis of spectra. A multivariate curve resolution was done on absorption and emission spectra of **FNP1$_{FA}$** and **FNP1$_{BOD\text{-}FA}$** recorded at all pH. For **FNP1$_{FA}$** the mathematical treatment found three absorption spectra (Figure S16) which closely match those of the neutral, anionic and dianionic forms of FA. Furthermore, the evolution of the concentration of the three species as a function of pH closely matches the reported one.[30] The same treatment on the absorption spectra of **FNP1$_{BOD\text{-}FA}$** (Figure S17) yields four contributions: the same three as the ones found for **FNP1$_{FA}$** which correspond to the FA in its three possible forms in the pH range studied and one which perfectly matches the BODIPY absorption spectrum. This last contribution is almost constant with pH.

A similar analysis on the emission spectra gave mixed results (Figure S18). The analysis of **FNP1$_{FA}$** yielded three components. But only two forms of the FA are known to emit fluorescence: the anion and dianion. The calculated spectra do not match the reported ones of the two forms.[30] The analysis of **FNP1$_{BOD\text{-}FA}$** yielded four components: the same three found for **FNP1$_{FA}$** and an additional one corresponding the BODIPY. Despite the fact that the FA contributions to the emission spectra does not totally match, the one of the BODIPY is satisfactory. Furthermore, its contribution is constant at all pH. It is thus reasonable to conclude that in the **FNP$_{BOD\text{-}FA}$** the spectral variations are solely due to the FA and that the BODIPY acts as

an internal reference. Therefore, despite the spectral overlap, it is possible to use it for a fluorescence ratiometric determination of the pH.

Ratiometric pH nanosensor

It was thus possible to realize a ratiometric pH titration with both types of FNP. The fluorescence ratio between the FA fluorescence emission recorded at 515 nm and the BODIPY one at 542 nm (F_{515}/F_{542}) was plotted against pH (right graphs in Figure 2 and Figure S12). Both curves fitted very well with the modified Henderson-Hasselbach equation:

$$I = \frac{I_A + I_B K_a 10^{pH}}{1 + K_a 10^{pH}} \qquad (2)$$

where I_A and I_B are respectively the ratio of fluorescent intensity (F_{515}/F_{542}) in acid and basic media and K_a is the acid dissociation constant (inflection point). This equation was used to fi the titrations curves. As such, pK_a were determined using the fitting parameters of equation 2.

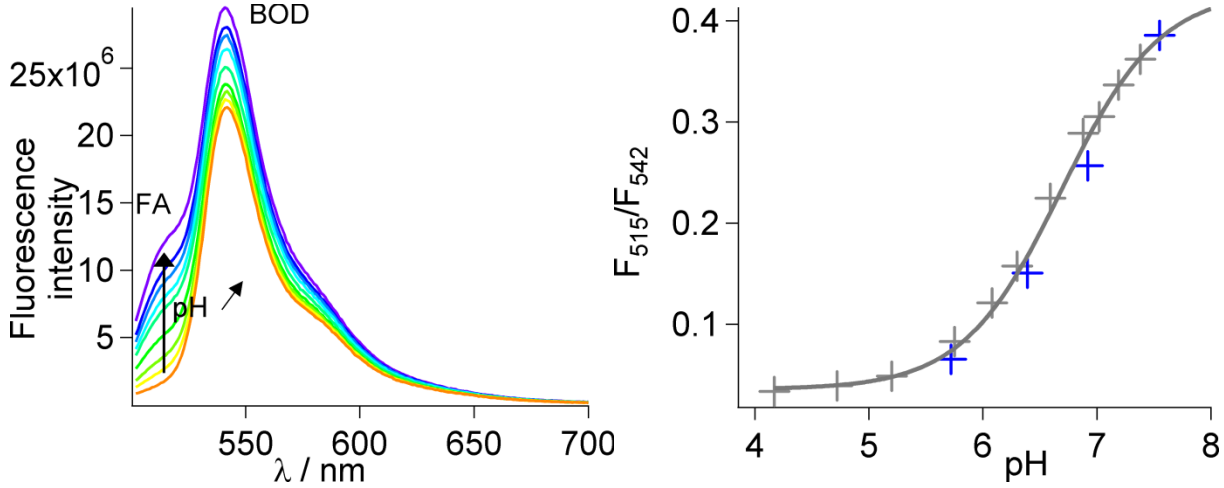

Fig. 2 Left: fluorescence emission spectra of **FNP1$_{BOD-FA}$** at various pH (λ_{exc} = 495 nm; phosphate/citrate buffers 10mM in 140mM NaCl; pH values: 8.01, 7.38, 7.19, 7.02, 6.88, 6.59, 6.3, 6.08, 5.75, 5.2, 4.72, 4.17); right: variation of the ratio of fluorescence intensity at 515 and 542 nm as a function of the pH (+) and fit using the Henderson-Hasselbach equation 2 with pK_a=6.69±0.04 (—). Grey points correspond to a decrease in pH and blue ones to an increase.

For **FNP1$_{BOD-FA}$** a pK_a = 6.69±0.04 was determined and for **FNP2$_{BOD-FA}$**, pK_a=6.47±0.04. Both pK_a were close to the one found for **FNP1$_{FA}$** and **FNP2$_{FA}$** nanoparticles (6.55±0.02; see above). Both systems showed excellent reversibility (compare blue *vs.* grey points on the graphs in Figure 2 and Figure S12). However, the overall fluorescence quantum yield of both nanoparticles types was rather low, which was previously attributed to a detrimental effect of the grafting reaction. Yet, the most important parameter to be considered for biological imaging is the brightness of the fluorescent nanoobjects. It was estimated considering a common 495 nm excitation wavelength and using the equation:

$$B = (\varepsilon_{FA}^{495} \times N_{FA} + \varepsilon_{BOD}^{495} \times N_{BOD}) \times \Phi_F \qquad (3)$$

where ε_{BOD}^{495} is the molar absorption coefficient of BODIPY at 495 nm (24800 $M^{-1}.cm^{-1}$), ε_{FA}^{495} is the molar absorption coefficient of grafted fluoresceinamine at 495 nm and pH 8 (88000 $M^{-1}.cm^{-1}$), Φ_F the fluorescent quantum yield of the nanoparticles when excited at 495 nm and N_{BOD} and N_{FA} the number of BODIPY and FA per particle (Table 1).

For both core-shell pH-sensitive fluorescent nanoparticles, the brightness was found to be 1.2×10^7 $M^{-1}.cm^{-1}$ which is very high compared to usual fluorescent nanoparticles (approximately 100 times brighter)[47-49] and 100 to 1000 brighter than the usual quantum dots.[50]

A linear variation of the ratio of the fluorescence intensities was obtained between pH 5.5 and 7.5 (Figures S11 and S12) which defined the useful range of measurable pH. The fluorescence intensities ratios (*i.e.* $([F_{515}/F_{542}]_{max})/([F_{515}/F_{542}]_{min})$) had an amplitude of 14 and 7 for **FNP1$_{BOD-FA}$** and **FNP2$_{BOD-FA}$** respectively. The smaller variation for **FNP2$_{BOD-FA}$** came from the lower amount of grafted FA. To the best of our knowledge, these values are higher than those reported to date for similar pH sensing and ratiometric polymer nanoparticles containing fluorescein.[7, 16-18, 21, 23]

It can thus be concluded that both types of **FNP$_{BOD-FA}$** are excellent pH ratiometric nanosensors due to their original design. Thanks to the location of the sensing dye and the reference dye in different regions of the nanoparticle, a single excitation wavelength can be used without significant cross talking (*i.e.* energy transfer) between the two fluorophores. In addition, the larger number of dyes incorporated in our FNP compared to previously reported ones makes them much brighter. All these properties lead to a large modulation of the fluorescence ratio upon pH variation: in the case of **FNP1$_{BOD-FA}$**, a variation of the F_{515}/F_{542} ratio of 1 corresponds to 0.14 pH unit in the operating range (5.5<pH<7.5) allowing a very precise determination of the pH.

Conclusions

A new ratiometric fluorescent pH nanosensor was designed and characterized. It was based on tailor-made ultrabright nanoparticles containing BODIPY fluorophores. They were readily synthesized using a one-pot procedure and post-functionalized with fluoresceinamine (FA). The nanoparticles were colloidally stable above pH=4, and contained a very large number of both fluorescent species (>2500). Their spectroscopic characteristics were fully studied in water at various pH, and the pK_a of the grafted fluorescein was determined to be close to the tabulated one. Furthermore, pH could be precisely measured between 5.5 and 7.5 thanks to a large variation of the fluorescence intensity ratio of the sensor FA to the reference dye BODIPY. In this system, no energy transfer from FA to BODIPY could be detected. Such non-FRET systems are highly robust to sense pH *in vivo* since there is no disturbing signal stemming from the environment of the dye. Indeed, a variation of ionic strength for example can change the conformation of polymer chains and as such the distance between the two dyes, resulting ultimately in a change in the FRET signal. The design of the nanoparticles allows for future developments, such as modulation of the nature of the copolymerized dye and the sensing one to expand their applicability. For example, it should be possible to replace the FA by sensors for heavy metal ions, and the BODIPY by near infrared dyes, to improve the spectral separation of the reference and sensing fluorophores. These modifications are currently under development in our laboratory.

Conflicts of interest

There are no conflicts to declare.

Acknowledgements

The authors would like to thanks Pr Bernadette Charleux for all the discussions on NPs synthesis, Sabrina Hocine and Min-Hui Li from Institut Curie (Paris, France) for the zeta potential measurements, Patricia Beaunier from Sorbonne Université (Paris, France) for the TEM images and Arnaud Brosseau (ENS Cachan, France) for spectroscopic measurement support.

Notes and references

1. C. McDonagh, C. S. Burke and B. D. MacCraith, *Chemical Reviews*, 2008, **108**, 400-422.
2. H. Qazi, A. Mohammad and M. Akram, *Sensors*, 2012, **12**, 16522.
3. S. T. Whitten, B. García-Moreno E. and V. J. Hilser, *Proceedings of the National Academy of Sciences of the United States of America*, 2005, **102**, 4282-4287.
4. J. R. Griffiths, *British journal of cancer*, 1991, **64**, 425-427.
5. L. Yuan, W. Lin, K. Zheng, L. He and W. Huang, *Chemical Society Reviews*, 2013, **42**, 622-661.
6. T. Terai and T. Nagano, *Current Opinion in Chemical Biology*, 2008, **12**, 515-521.
7. J. E. Whitaker, R. P. Haugland and F. G. Prendergast, *Analytical Biochemistry*, 1991, **194**, 330-344.
8. J. Han and K. Burgess, *Chemical Reviews*, 2010, **110**, 2709-2728.
9. H. Koo, M. S. Huh, J. H. Ryu, D.-E. Lee, I.-C. Sun, K. Choi, K. Kim and I. C. Kwon, *Nano Today*, 2011, **6**, 204-220.
10. N. Hildebrandt, C. M. Spillmann, W. R. Algar, T. Pons, M. H. Stewart, E. Oh, K. Susumu, S. A. Díaz, J. B. Delehanty and I. L. Medintz, *Chemical Reviews*, 2017, **117**, 536-711.
11. S. Sharifi, S. Behzadi, S. Laurent, M. Laird Forrest, P. Stroeve and M. Mahmoudi, *Chemical Society Reviews*, 2012, **41**, 2323-2343.
12. S. Bonacchi, D. Genovese, R. Juris, M. Montalti, L. Prodi, E. Rampazzo and N. Zaccheroni, *Angewandte Chemie International Edition*, 2011, **50**, 4056-4066.
13. S. W. Bae, W. Tan and J.-I. Hong, *Chemical Communications*, 2012, **48**, 2270-2282.
14. C. Li and S. Liu, *Chemical Communications*, 2012, **48**, 3262-3278.
15. T. Doussineau, A. Schulz, A. Lapresta-Fernandez, A. Moro, S. Körsten, S. Trupp and G. J. Mohr, *Chemistry – A European Journal*, 2010, **16**, 10290-10299.
16. H. Sun, K. Almdal and T. L. Andresen, *Chemical Communications*, 2011, **47**, 5268-5270.
17. R. V. Benjaminsen, H. Sun, J. R. Henriksen, N. M. Christensen, K. Almdal and T. L. Andresen, *ACS Nano*, 2011, **5**, 5864-5873.
18. E. Allard and C. Larpent, *Journal of Polymer Science Part A: Polymer Chemistry*, 2008, **46**, 6206-6213.
19. S. Hornig, C. Biskup, A. Gräfe, J. Wotschadlo, T. Liebert, G. J. Mohr and T. Heinze, *Soft Matter*, 2008, **4**, 1169-1172.
20. A. Schulz, J. Wotschadlo, T. Heinze and G. J. Mohr, *Journal of Materials Chemistry*, 2010, **20**, 1475-1482.
21. H. Sun, A. M. Scharff-Poulsen, H. Gu and K. Almdal, *Chemistry of Materials*, 2006, **18**, 3381-3384.
22. C. Li, Y. Zhang, J. Hu, J. Cheng and S. Liu, *Angewandte Chemie International Edition*, 2010, **49**, 5120-5124.
23. K. Ouadahi, K. Sbargoud, E. Allard and C. Larpent, *Nanoscale*, 2012, **4**, 727-732.
24. H.-s. Peng, J. A. Stolwijk, L.-N. Sun, J. Wegener and O. S. Wolfbeis, *Angewandte Chemie International Edition*, 2010, **49**, 4246-4249.
25. J. Chen, Y. Tang, H. Wang, P. Zhang, Y. Li and J. Jiang, *Journal of Colloid and Interface Science*, 2016, **484**, 298-307.
26. P. Zhang, H. Wang, Y. Hong, M. Yu, R. Zeng, Y. Long and J. Chen, *Biosensors and Bioelectronics*, 2018, **99**, 318-324.
27. M. Ryvolova, J. Chomoucka, J. Drbohlavova, P. Kopel, P. Babula, D. Hynek, V. Adam, T. Eckschlager, J. Hubalek, M. Stiborova, J. Kaiser and R. Kizek, *Sensors (Basel, Switzerland)*, 2012, **12**, 14792-14820.
28. C. Grazon, J. Rieger, R. Méallet-Renault, G. Clavier and B. Charleux, *Macromolecular Rapid Communications*, 2011, **32**, 699-705.
29. C. Grazon, J. Rieger, R. Méallet-Renault, B. Charleux and G. Clavier, *Macromolecules*, 2013, **46**, 5167-5176.
30. R. Sjöback, J. Nygren and M. Kubista, *Spectrochimica Acta Part A: Molecular and Biomolecular Spectroscopy*, 1995, **51**, L7-L21.
31. C. Munkholm, D. R. Parkinson and D. R. Walt, *Journal of the American Chemical Society*, 1990, **112**, 2608-2612.
32. D. H. Ma, D. Kim, T. Akisawa, K.-H. Lee, K.-T. Kim and K. H. Ahn, *Chemistry – An Asian Journal*, 2015, **10**, 894-902.
33. L. Couvreur, C. Lefay, J. Belleney, B. Charleux, O. Guerret and S. Magnet, *Macromolecules*, 2003, **36**, 8260-8267.
34. R. Birge, *Kodak laser dyes*, Eastman Kodak Company, Rochester, NY, 1987.
35. B. Valeur and M. N. Berberan-Santos, *Molecular fluorescence: principles and applications*, John Wiley & Sons, 2012.
36. S. Boissé, J. Rieger, K. Belal, A. Di-Cicco, P. Beaunier, M.-H. Li and B. Charleux, *Chemical Communications*, 2010, **46**, 1950-1952.
37. C. Grazon, J. Rieger, P. Beaunier, R. Méallet-Renault and G. Clavier, *Polymer Chemistry*, 2016, **7**, 4272-4283.
38. J. B. McLeary and B. Klumperman, *Soft Matter*, 2006, **2**, 45-53.
39. P. B. Zetterlund, Y. Kagawa and M. Okubo, *Chemical Reviews*, 2008, **108**, 3747-3794.
40. Y. Si, C. Grazon, G. Clavier, J. Rieger, J.-F. Audibert, B. Sclavi and R. Méallet-Renault, *Biosensors and Bioelectronics*, 2016, **75**, 320-327.
41. C. A. G. N. Montalbetti and V. Falque, *Tetrahedron*, 2005, **61**, 10827-10852.
42. F. A. Tobiesen and S. Michielsen, *Journal of Polymer Science Part A: Polymer Chemistry*, 2002, **40**, 719-728.
43. S. Yang, X. Yu, L. Wang, Y. Tu, J. X. Zheng, J. Xu, R. M. Van Horn and S. Z. D. Cheng, *Macromolecules*, 2010, **43**, 3018-3026.
44. A. Ranjan, N. Pothayee, M. Seleem, N. Jain, N. Sriranganathan, J. S. Riffle and R. Kasimanickam, *Journal of Nanoparticle Research*, 2010, **12**, 905-914.
45. M. Carvell, I. D. Robb and P. W. Small, *Polymer*, 1998, **39**, 393-398.
46. C. Déjugnat, D. Haložan and G. B. Sukhorukov, *Macromolecular Rapid Communications*, 2005, **26**, 961-967.
47. A. Reisch and A. S. Klymchenko, *Small*, 2016, **12**, 1968-1992.
48. G. Sun, M. Y. Berezin, J. Fan, H. Lee, J. Ma, K. Zhang, K. L. Wooley and S. Achilefu, *Nanoscale*, 2010, **2**, 548-558.

49. R. Méallet-Renault, A. Hérault, J.-J. Vachon, R. B. Pansu, S. Amigoni-Gerbier and C. Larpent, *Photochemical & Photobiological Sciences*, 2006, **5**, 300-310.
50. U. Resch-Genger, M. Grabolle, S. Cavaliere-Jaricot, R. Nitschke and T. Nann, *Nature Methods*, 2008, **5**, 763.

Supporting Information

Core-shell polymeric nanoparticles comprising BODIPY and fluorescein as ultra-bright ratiometric fluorescent pH sensors

C. Grazon,*[a]† Y. Si,[a] J.-P. Placial,[a] J. Rieger,[b] R. Méallet-Renault[a,]§ and G. Clavier[a]

[a] PPSM, ENS Cachan, CNRS, Université Paris-Saclay, 94235 Cachan, France

E-mail: chloe.grazon@u-bordeaux.fr

[b] Sorbonne Université, CNRS, Institut Parisien de Chimie Moléculaire, UMR 8232, Team : Chimie des Polymères, 75005 Paris, France.

Current addresses:

† Laboratoire de Chimie des Polymères Organiques (LCPO), CNRS UMR 5629, Université de Bordeaux, Bordeaux-INP, Pessac 33607 Cedex, France.

§ Institut des Sciences Moléculaires d'Orsay (ISMO), CNRS, Univ. Paris-Sud, Université Paris-Saclay, F-91405 Orsay (France).

Equations

The aggregation number N_{agg} was calculated using the equation:

$$N_{agg} = \frac{n_{chain}}{n_{FNP}} = \frac{V_{FNP}}{V_S} \times n_{chain} = \frac{\frac{4}{3}\pi r^3}{m_S \rho_S} \times n_{chain} \quad \text{(S1)}$$

$$N_{agg} = \frac{n_{chain}}{n_{FNP}} = \frac{V_S}{V_{FNP}} * n_{chain} = \frac{mS_\rho}{\frac{4}{3}\pi r^3} * n_{chain}$$

where n_{chain} is the total number of growing chains (which is equal to the number of macroRAFT agent assuming they are all incorporated in the nanoparticles), n_{FNP} is the number of fluorescent nanoparticles, V_S the total volume of styrene in the synthesis, V_{FNP} is the volume of one fluorescent nanoparticle, m_S the total mass of styrene in the synthesis, ρ_S the polystyrene density and r the core radius of the nanoparticles determined by TEM microscopy (Figure S1).

The number of BODIPY monomer (η_{BOD}) per polymer chain was calculated using the equation:

$$\eta_{BOD} = \frac{n_{BOD}}{n_{RAFT}} \quad \text{(S2)}$$

where n_{BOD} and n_{RAFT} are respectively the moles number of BOD and macroRAFT agent used in the nanoparticles synthesis.

The number of BODIPY monomer (N_{BOD}) per FNP was calculated using the equation:

$$N_{BOD} = N_{agg} \times \eta_{BOD} \quad \text{(S3)}$$

The brightness (B) of the FNP containing only one type of dye was calculated using the equation:

$$B = \varepsilon_\lambda \times N \times \Phi_F \quad \text{(S4)}$$

Where ε_λ is the molar absorption coefficient of the dye at the wavelength (λ) of excitation, Φ_F the fluorescent quantum yield of the nanoparticles and N the number of dyes per nanoparticle.

Synthesis of FNP

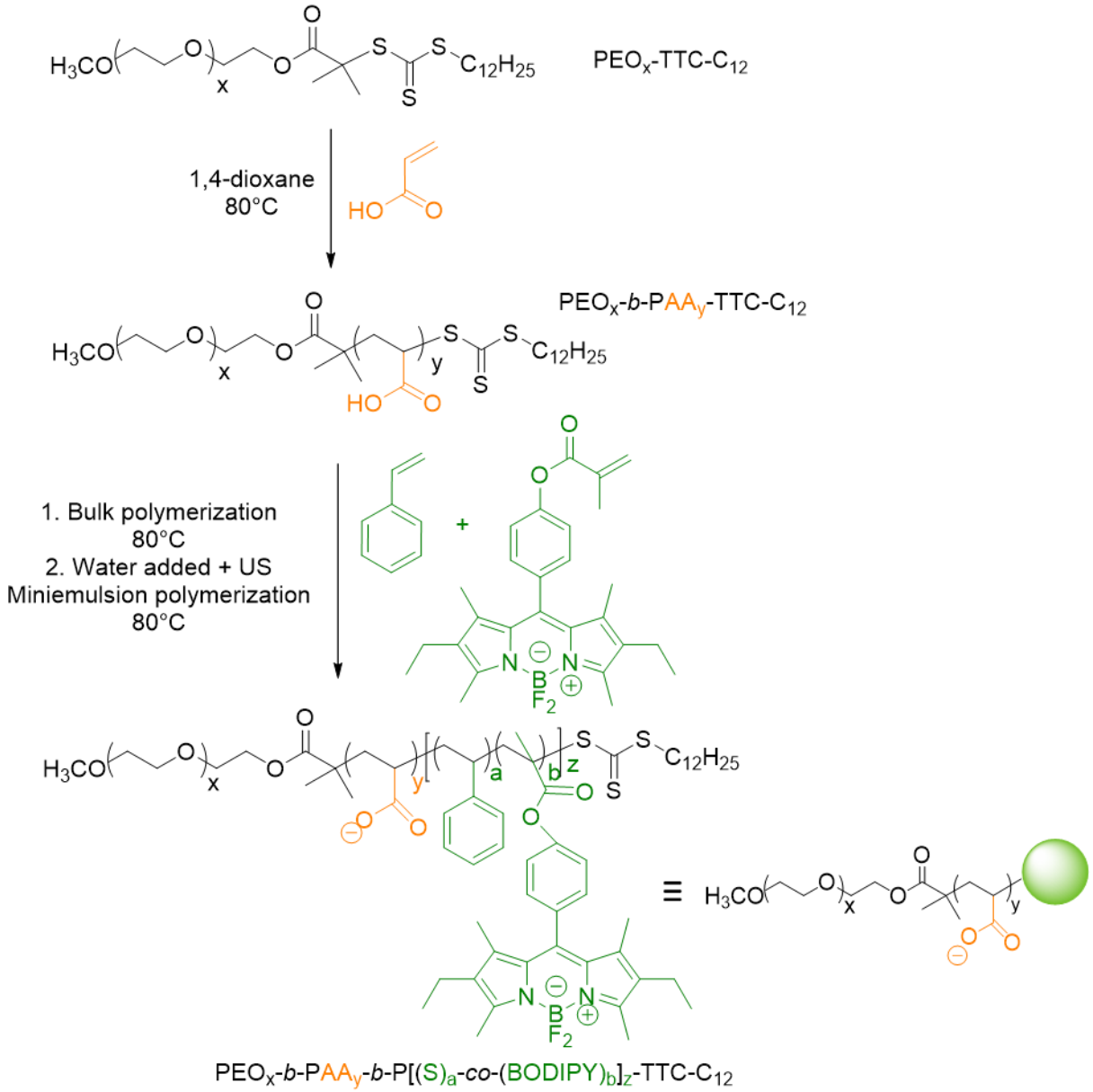

Scheme S1. Synthetic scheme employed for the synthesis of the fluorescent nanoparticles **FNP1$_{BOD}$** stabilized by a double hydrophilic block copolymer (PEO-*b*-PAA shell).

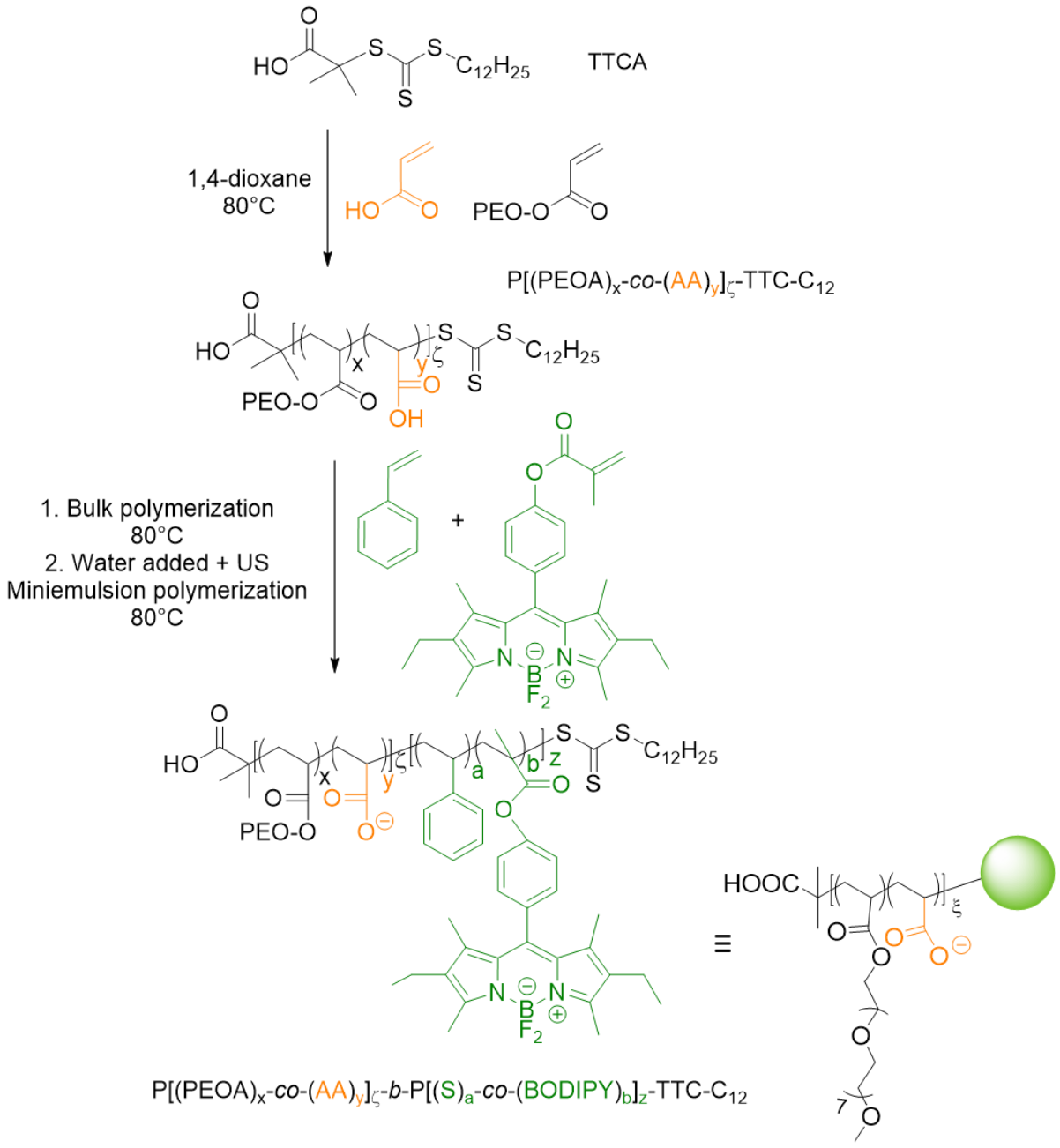

Scheme S2. Synthetic scheme employed for the synthesis of the fluorescent nanoparticles **FNP2$_{BOD}$** stabilized by a hydrophilic random copolymer (P(PEOA-*co*-AA) shell).

Table S1. Characterization of fluorescent nanoparticles (FNP) having different shells, synthesized *via* a one-pot miniemulsion polymerization.

Sample	shell	n_{BOD}[a]	conv.$_S$[b]	conv.$_{BOD}$[c]	$M_{n,th}$ [kg/mol] [d]	$M_{n,SEC}$ [kg/mol] [e]	M_w/M_n[e]	D_h (σ)[f] nm
FNP1$_{BOD}$	PEO_{45}-*b*-PAA_{15}	1.1	0.91	0.99	15.2	23.7	1.45	76 (0.12)
FNP1	PEO_{45}-*b*-PAA_{19}	0	0.97	-	14.2	16.8	1.29	80 (-)
FNP2$_{BOD}$	P($AA_{0.5}$-*co*-$PEOA_{0.5}$)$_{22}$	2.0	0.97	0.97	22.4	18.5	1.40	77 (0.10)
FNP2	P($AA_{0.5}$-*co*-$PEOA_{0.5}$)$_{22}$	0	0.85	-	19.7	17.1	1.35	70 (0.12)

[a] Average number of BODIPY per polymer chain (with a $DP_{n,total}$ about 120), calculated using eq. S2. [b] Styrene conversion determined by gravimetry. [c] BODIPY conversion determined by SEC by comparison of the calculated area of the polymer and monomer peaks from SEC equipped with a UV-vis detector (C. Grazon, *et al*. *Macromol. Rapid Commun.* 2011, **32**, 699). [d] Theoretical number-average molar mass ($M_{n\,th} = M_{n\,CTA} + 1/n_{CTA} \times (conv._S \times m_S + conv._{BOD} \times m_{BOD})$, where CTA stands for chain transfer agent, conv.$_S$ and conv.$_{BOD}$ the individual conversion of styrene and BODIPY and m the mass of monomer used in the synthesis). [e] Number-average molar mass ($M_{n,SEC}$) and molar mass dispersity (M_w/M_n) determined by SEC using a polystyrene calibration. [f] Hydrodynamic diameter (D_h) and dispersity factor (σ) determined by DLS.

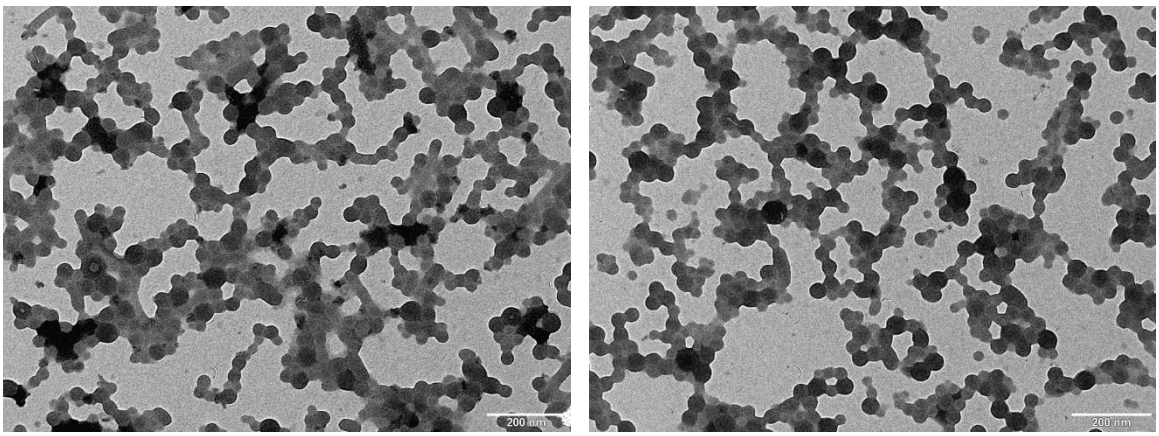

Figure S1. Transmission electron microscopy photographs of the dried fluorescent nanoparticles (scale bar: 200 nm). Left: **FNP1$_{BOD\text{-}FA}$** and right: **FNP2$_{BOD\text{-}FA}$**.

Spectroscopic characterizations of FNP_{BOD}

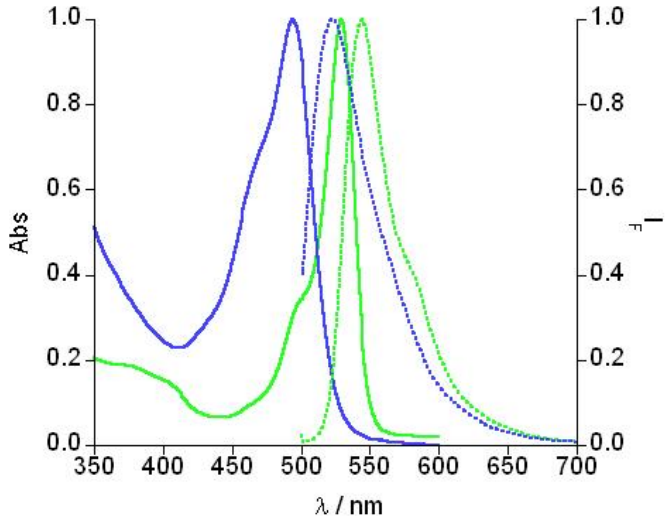

Figure S2. Normalized absorption (full lines) and fluorescence emission spectra (dotted lines, λ_{exc} = 495 nm) of **$FNP1_{BOD}$** (—) and **$FNP1_{FA}$** (—) at pH = 8.

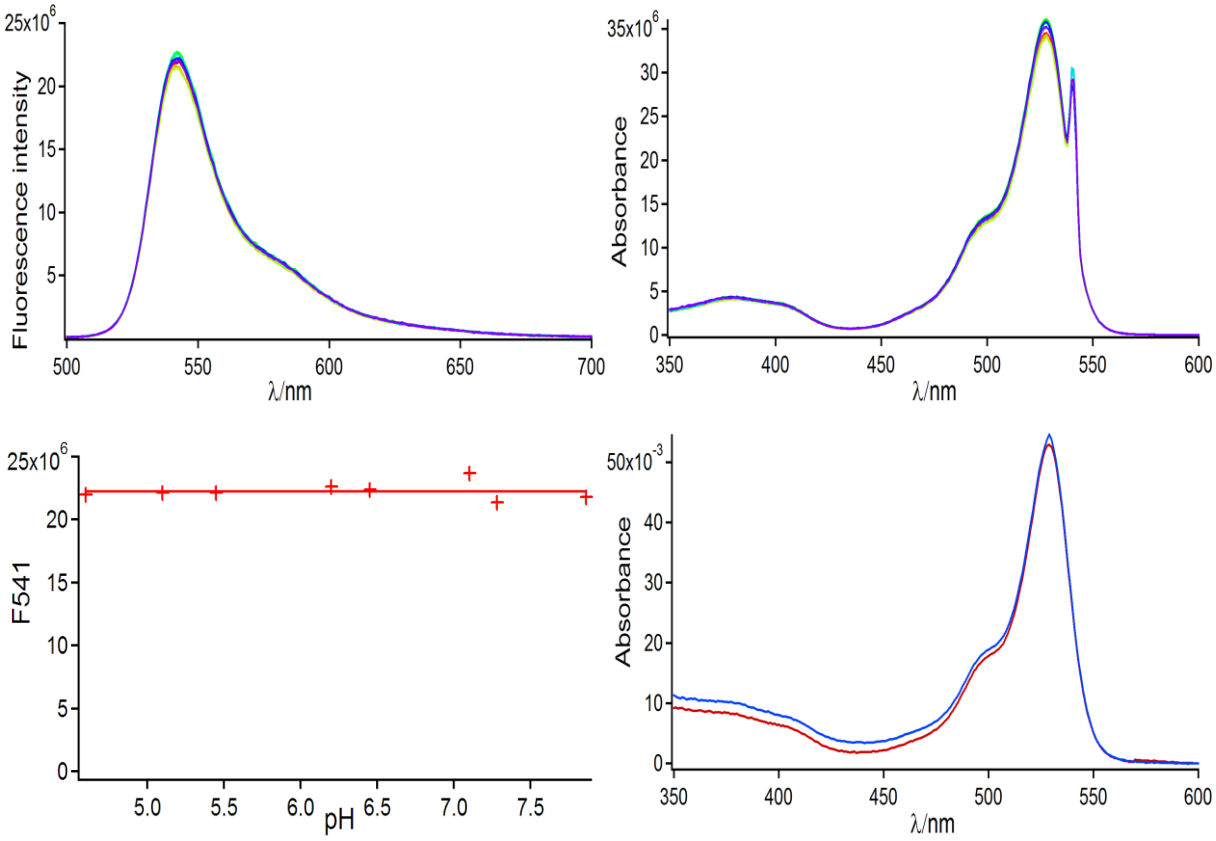

Figure S3. Top left: fluorescence emission spectra of **FNP1$_{BOD}$** at various pH (λ_{ex}=495nm); Top right: fluorescence excitation spectra of **FNP1$_{BOD}$** at various pH (λ_{em}=550nm). Bottom: variation of fluorescence intensity at 541nm as a function of the pH (+) and fit using a straight line. Conditions: phosphate/citrate buffers 1mM in 140mM NaCl; pH values: 7.86, 7.28, 7.10, 7.00, 6.45, 6.20, 5.45, 5.10, 4.60. Bottom right: absorption spectra (pH=4: red line, pH=8: blue line).

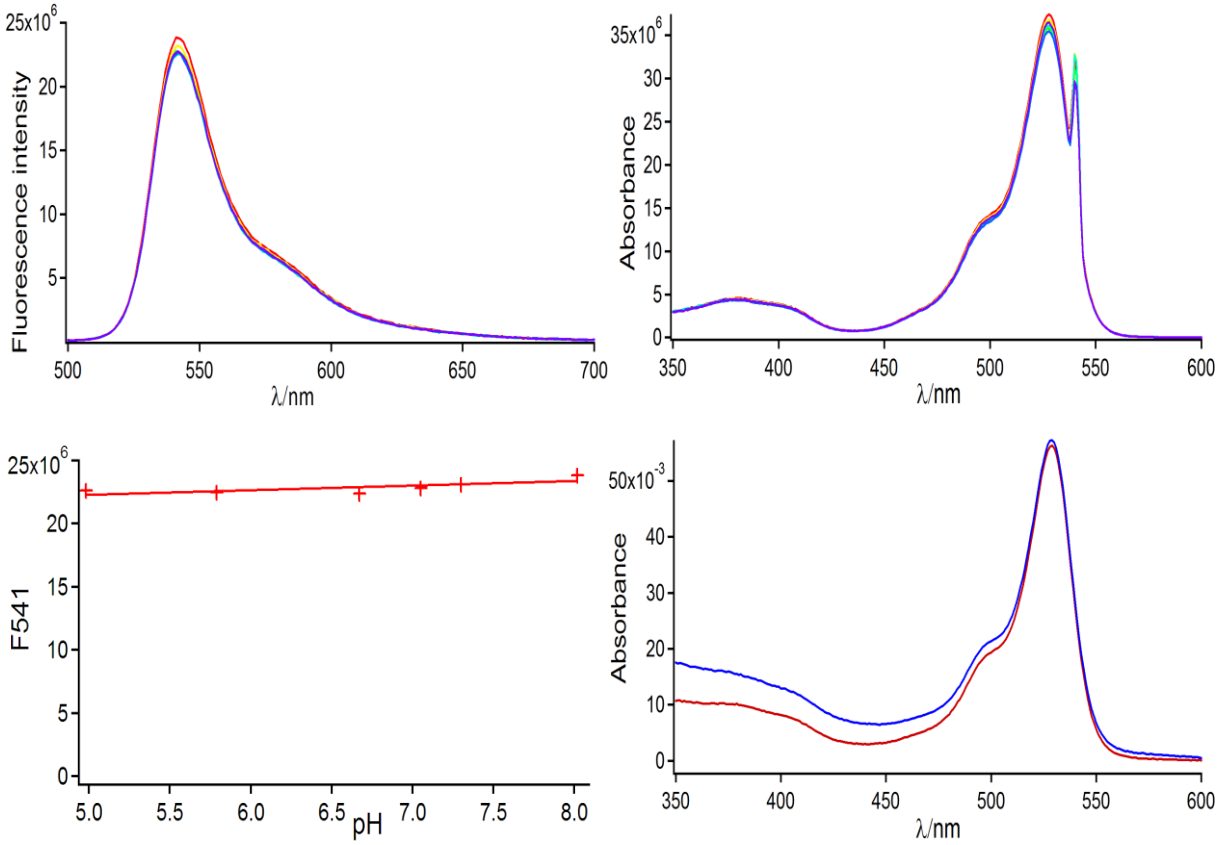

Figure S4. Top left: fluorescence emission spectra of **FNP1$_{BOD}$** at various pH (λ_{ex}=495nm); Top right: fluorescence excitation spectra of **FNP1$_{BOD}$** at various pH (λ_{em}=550nm). Bottom: variation of fluorescence intensity at 541nm as a function of the pH (+) and fit using a straight line. Conditions: phosphate/citrate buffers 10mM in 140mM NaCl; pH values: 8.02, 7.30, 7.05, 6.67, 5.79, 4.98. Bottom right: absorption spectra (pH=4: red line, pH=8: blue line).

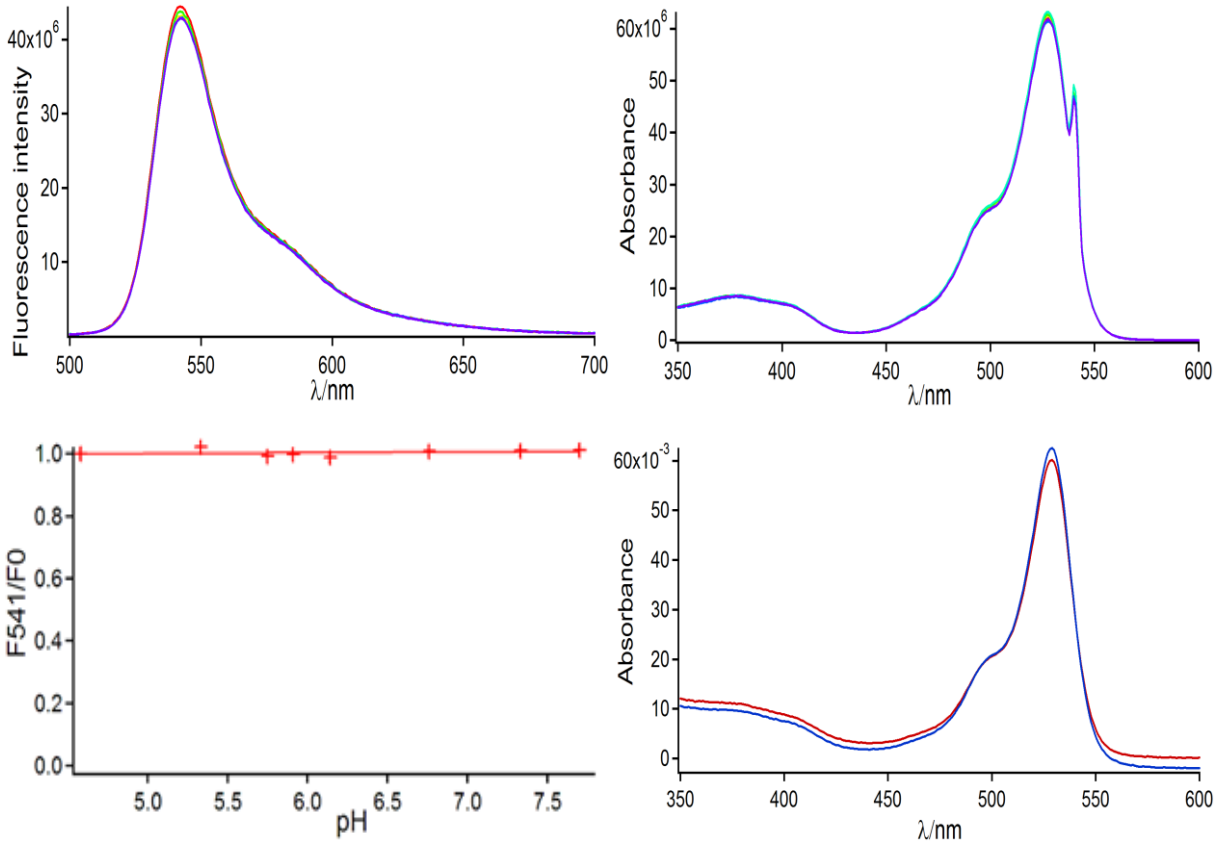

Figure S5. Top left: fluorescence emission spectra of **FNP2$_{BOD}$** at various pH (λ_{ex}=495nm); Top right: fluorescence excitation spectra of **FNP2$_{BOD}$** at various pH (λ_{em}=550nm). Bottom left: relative variation of fluorescence intensity at 541nm as a function of the pH (+) and fit using a straight line (F0: fluorescence intensity at 541nm when pH=4.58). Conditions: phosphate/citrate buffers 1mM in 140mM NaCl; pH values: 4.58, 5.33, 5.75, 5.91, 6.14, 6.76, 7.33 and 7.70. Bottom right: absorption spectra (pH=4: red line, pH=8: blue line).

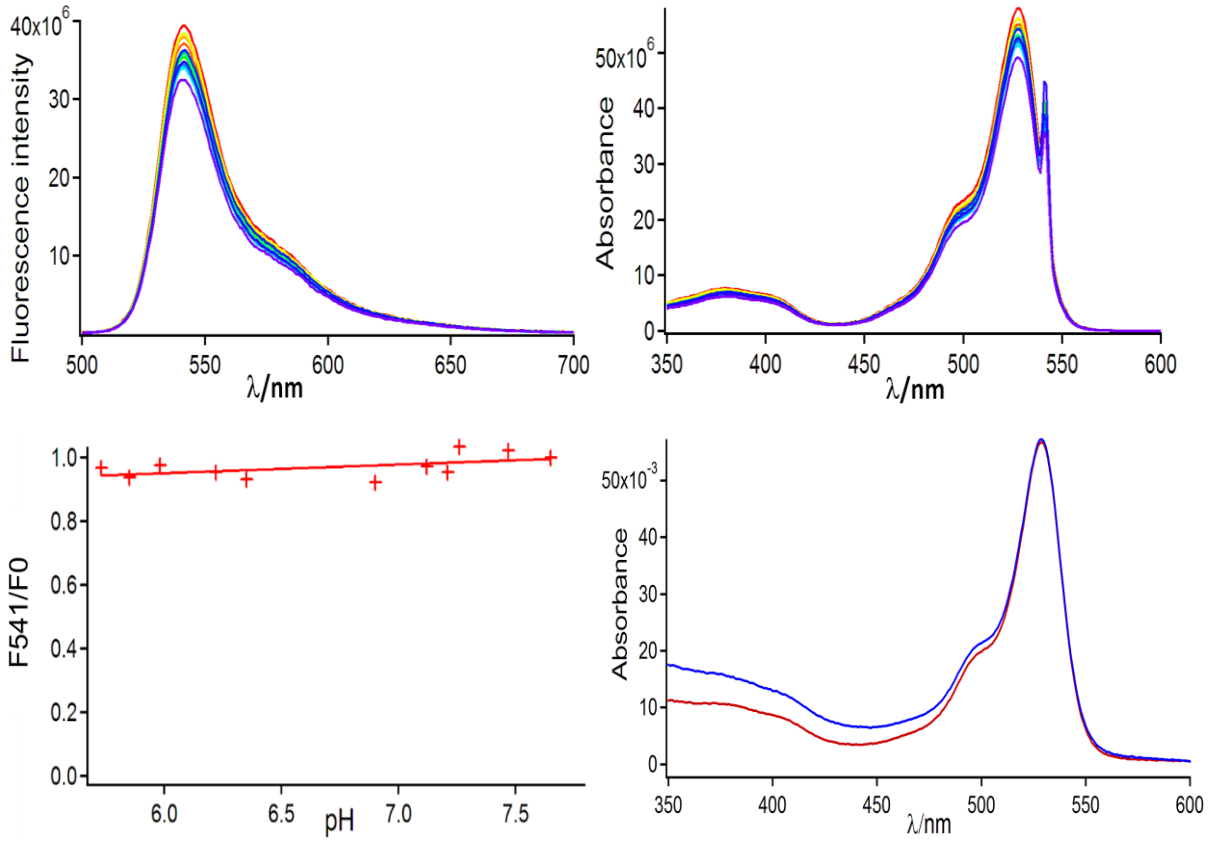

Figure S6. Top left: fluorescence emission spectra of **FNP2$_{BOD}$** at various pH (λ_{ex}=495nm); Top right: fluorescence excitation spectra of **FNP2$_{BOD}$** at various pH (λ_{em}=550nm). Bottom: relative variation of fluorescence intensity at 541nm as a function of the pH (+) and fit using a straight line (F0: fluorescence intensity at 541nm when pH=7.65). Conditions: phosphate/citrate buffers 10mM in 140mM NaCl; pH values: 7.65, 7.47, 7.26, 7.21, 7.12, 6.90, 6.35, 6.22, 5.98, 5.85, 5.73, 5.36. Bottom right: absorption spectra (pH=4: red line, pH=8: blue line).

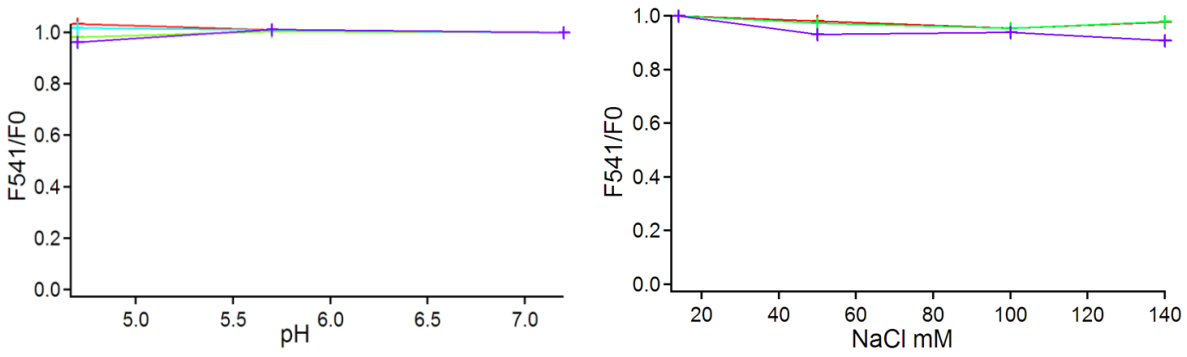

Figure S7. Left: relative variation of fluorescence intensity of **FNP1$_{BOD}$** at 541nm as a function of the pH in 1mM phosphate/citrate buffers and at various NaCl concentrations: 14 mM (red), 50 mM (green), 100 mM (blue) and 140 mM (purple); pH values: 4.7, 5.7 and 7.2. (F0: fluorescence intensity of **FNP1$_{BOD}$** at

541nm when pH=7.2). Right: relative variation of fluorescence intensity of **FNP1$_{BOD}$** at 541nm as a function of NaCl concentration in phosphate/citrate buffers 1mM and at various pH values: 4.7 (purple), 5.7 (green) and 7.2 (red); NaCl concentrations: 14mM, 50mM, 100mM and 140mM. (F0: fluorescence intensity of **FNP1$_{BOD}$** at 541nm when NaCl concentration= 14mM).

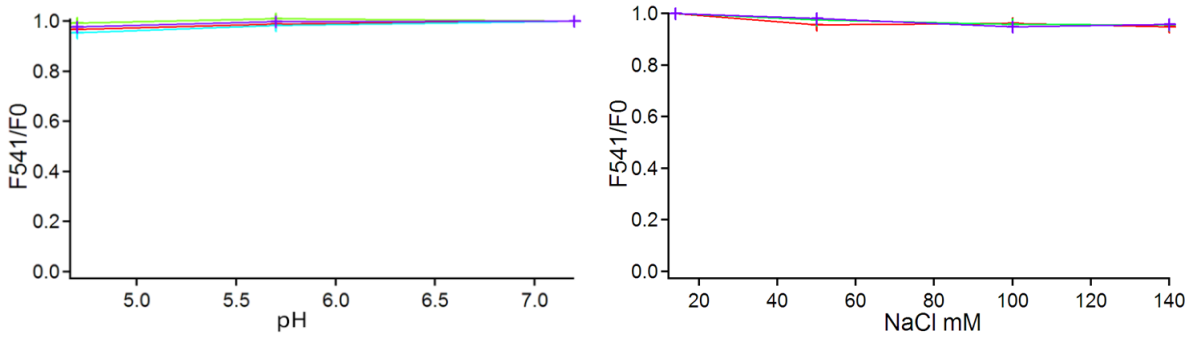

Figure S8. Left: relative variation of fluorescence intensity of **FNP2$_{BOD}$** at 541nm as a function of the pH in 1mM phosphate/citrate buffers and at various NaCl concentrations: 14 mM (red), 50 mM (green), 100 mM (blue) and 140 mM (purple) and fit using a straight line. pH values: 4.7, 5.7 and 7.2. (F0: fluorescence intensity of **FNP2$_{BOD}$** at 541nm when pH=7.2). Right: relative variation of fluorescence intensity of **FNP2$_{BOD}$** at 541nm as a function of NaCl concentration in 1mM phosphate/citrate buffers at various pH values: 4.7 (purple), 5.7 (green) and 7.2 (red); NaCl concentrations: 14mM, 50mM, 100mM and 140mM. (F0: fluorescence intensity of **FNP2$_{BOD}$** at 541nm when NaCl concentration= 14mM).

Spectroscopic characterizations of FNP_{FA}

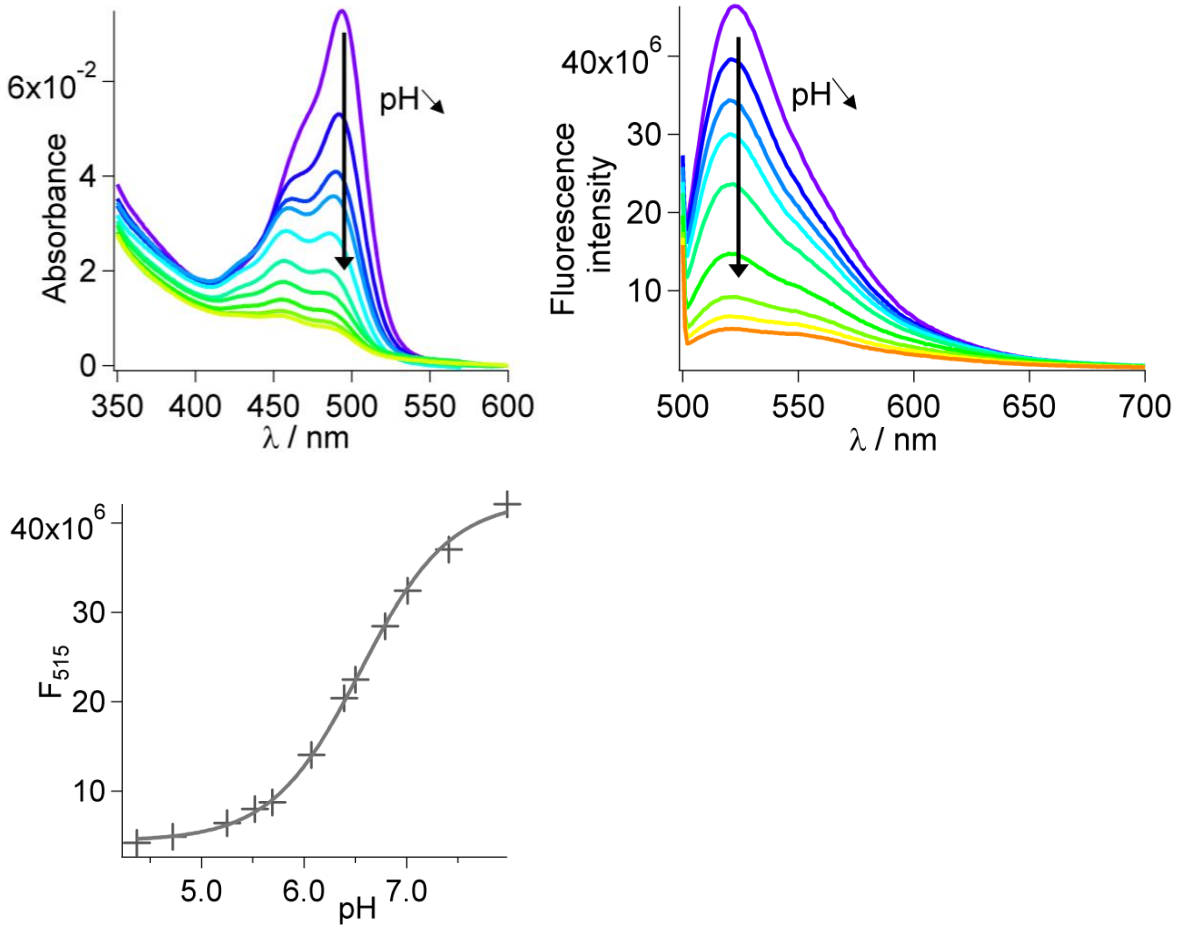

Figure S9. Top left: absorption spectra of **$FNP1_{FA}$** at various pH. Top right: fluorescence emission spectra of **$FNP1_{FA}$** at various pH (λ_{exc} = 495 nm). Bottom: variation of fluorescence intensity at 515 nm as a function of the pH (+) and fit using the Henderson-Hasselbach equation 2 with pKa = 6.55 (—). pH values: 7.98, 7.41, 7.01, 6.79, 6.50, 6.39, 6.07, 5.69, 5.52, 5.25, 4.72, 4.37.

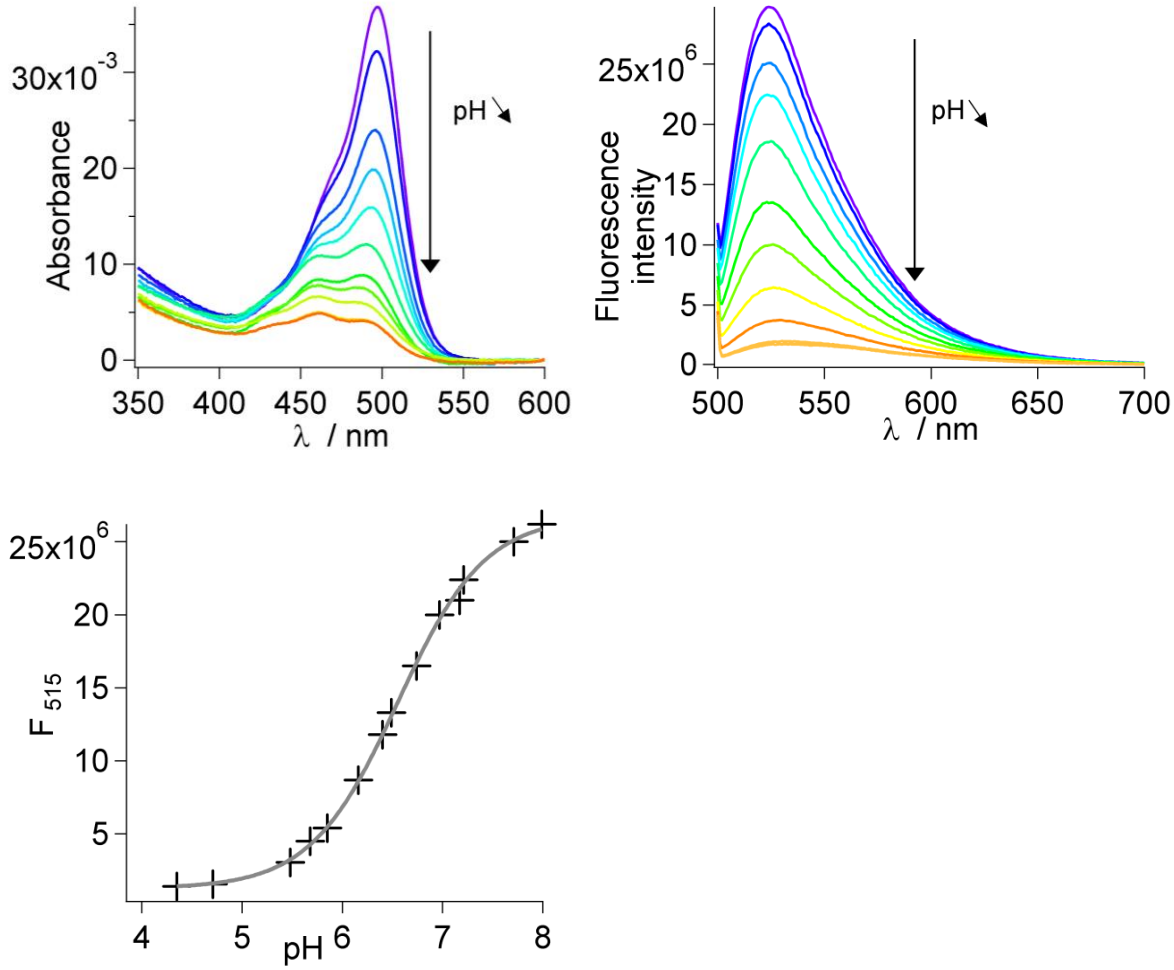

Figure S10. Top left: absorption spectra of **FNP2$_{FA}$** at various pH. Top right: fluorescence emission spectra of **FNP2$_{FA}$** at various pH (λ_{exc} = 495 nm). Bottom: variation of fluorescence intensity at 515 nm as a function of the pH (+) and fit using the Henderson-Hasselbach equation 2 with pKa = 6.55 (—). pH values: 7.99, 7.71, 7.21, 7.17, 6.97, 6.74, 6.49, 6.40, 6.16, 5.85, 5.68, 5.48, 4.71, 4.35.

Absorption and emission spectra of FNP_{BOD-FA} with pH

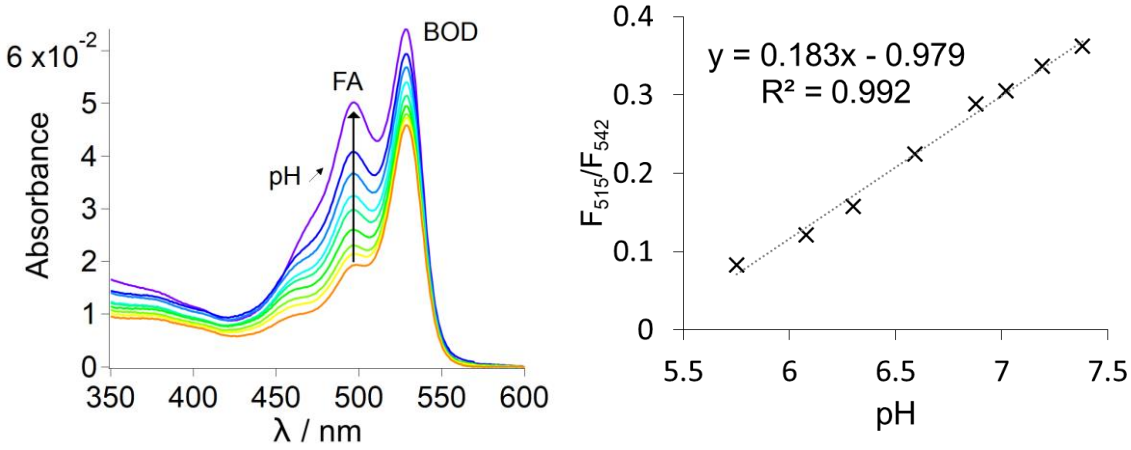

Figure S11. Left: absorption spectra of **$FNP1_{BOD-FA}$** at various pH (phosphate/citrate buffers 10mM in 140mM NaCl; pH values: 8.01, 7.38, 7.19, 7.02, 6.88, 6.59, 6.30, 6.08, 5.75). Right: variation of the ratio of fluorescence intensity at 515 and 542 nm as a function of the pH (between pH = 5.5 and 7.5) and fit using a linear equation.

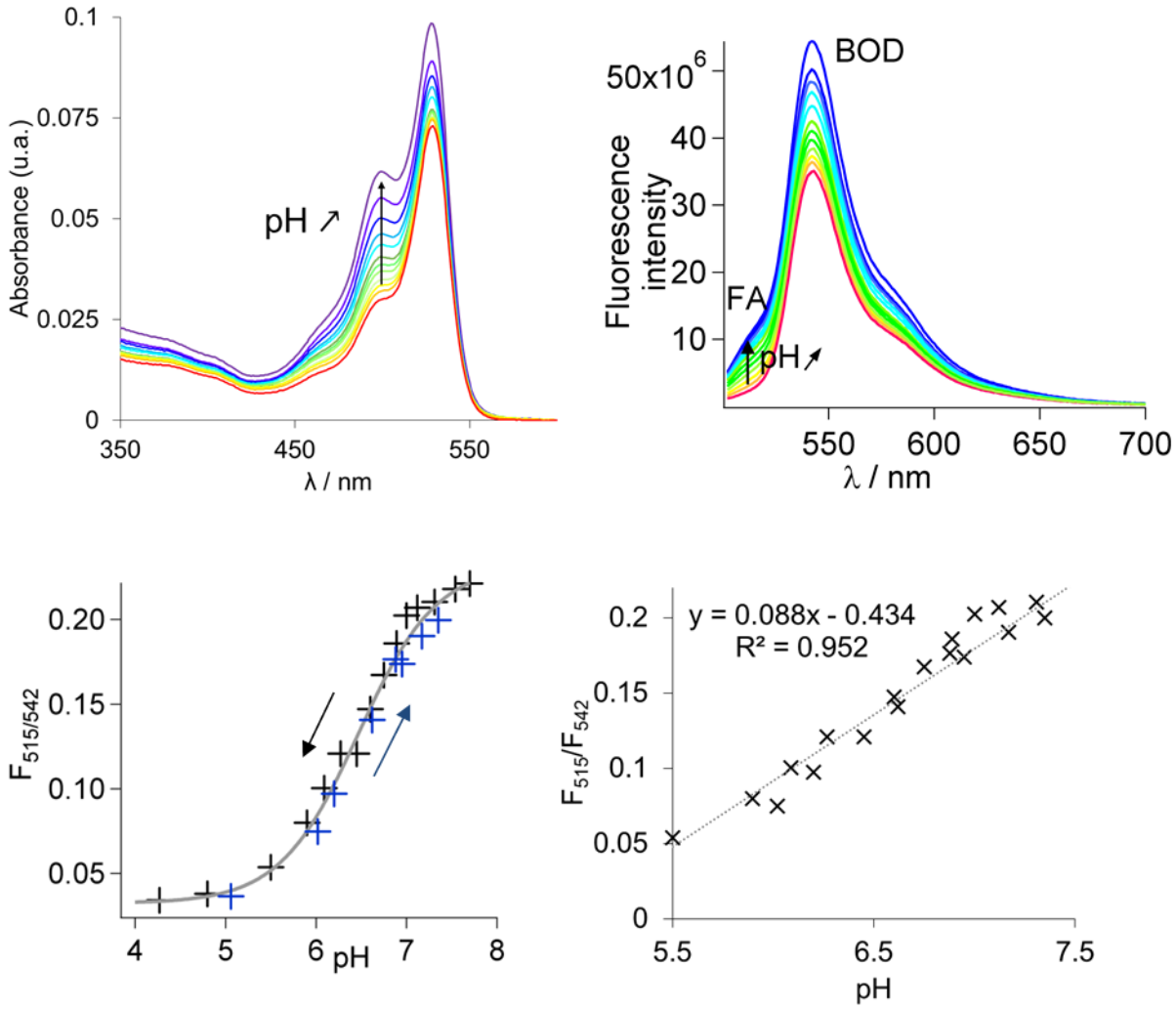

Figure S12. Spectra of **FNP2$_{BOD-FA}$** at various pH (λ_{exc} = 495 nm; phosphate/citrate buffers 10mM in 140mM NaCl; pH values: 7.70, 7.54, 7.31, 7.00, 6.89, 6.75, 6.60, 6.45, 6.27, 6.09, 5.90, 5.50, 4.80, 4.27). Top left: absorption. Top right: fluorescence emission (λ_{exc} = 495 nm. Bottom left: variation of the ratio of fluorescence intensity at 515 and 542 nm as a function of the pH (+) and fit using the Henderson-Hasselbach equation 2 with pK_a = 6.47 (—). Grey points correspond to a decrease in pH and blue ones to an increase. Bottom right: variation of the ratio of fluorescence intensity at 515 and 542 nm as a function of the pH (between pH = 5.5 and 7.5) and fit using a linear equation.

Excitation spectra of all FNP

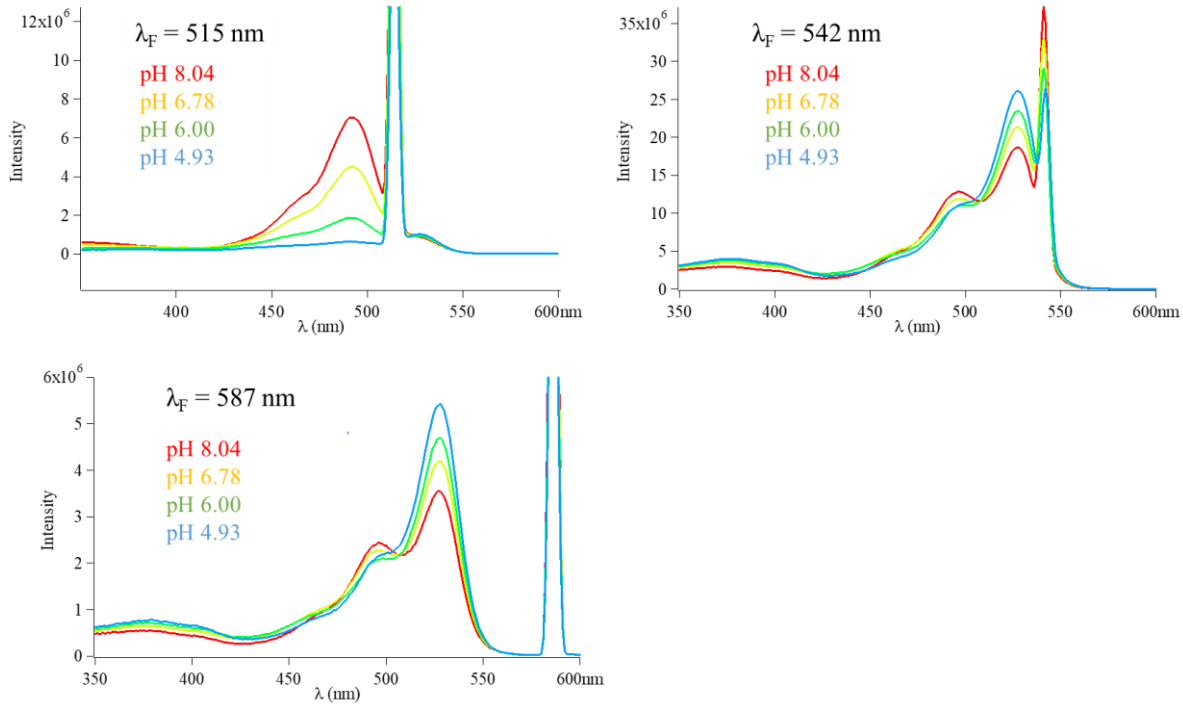

Figure S13 Excitation spectra of FNP1$_{BOD\text{-}FA}$ recorded at 3 different emission wavelengths (λ_F = 515, 542 or 587 nm) and at 4 different pH (8.04, 6.78, 6.00, 4.93).

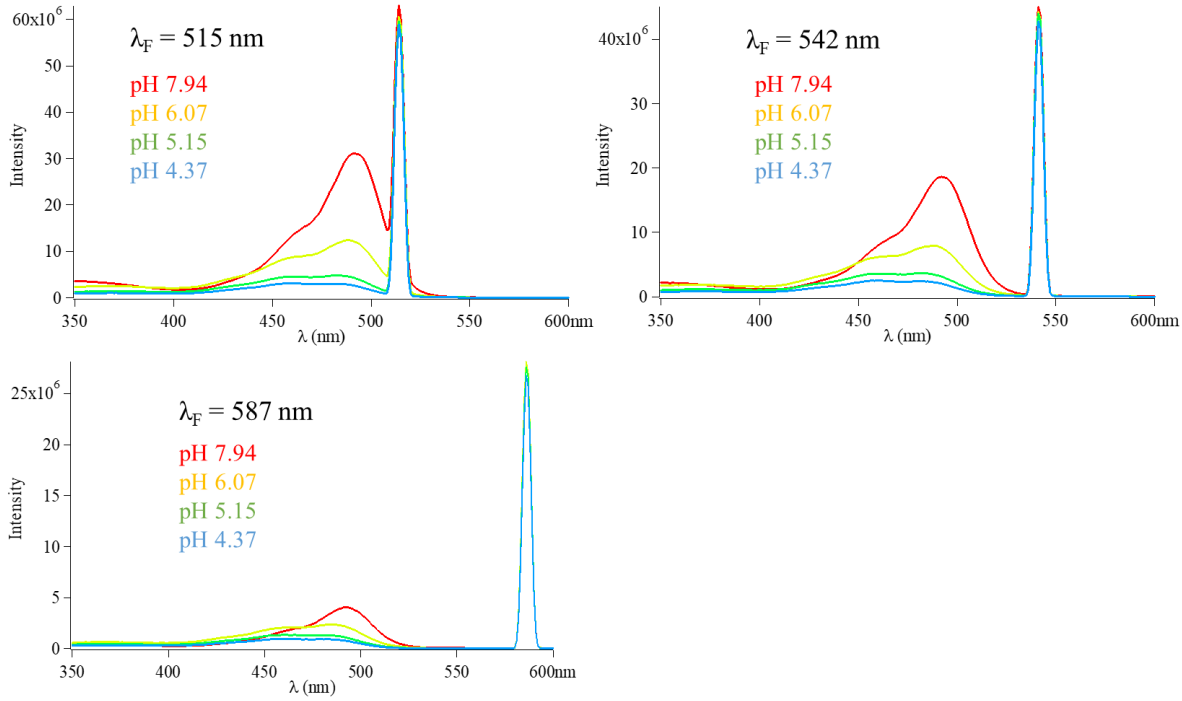

Figure S14 Excitation spectra of $FNP1_{FA}$ recorded at 3 different emission wavelengths (λ_F = 515, 542 or 587 nm) and at 4 different pH (7.94, 6.07, 5.15, 4.37).

Fluorescence decays

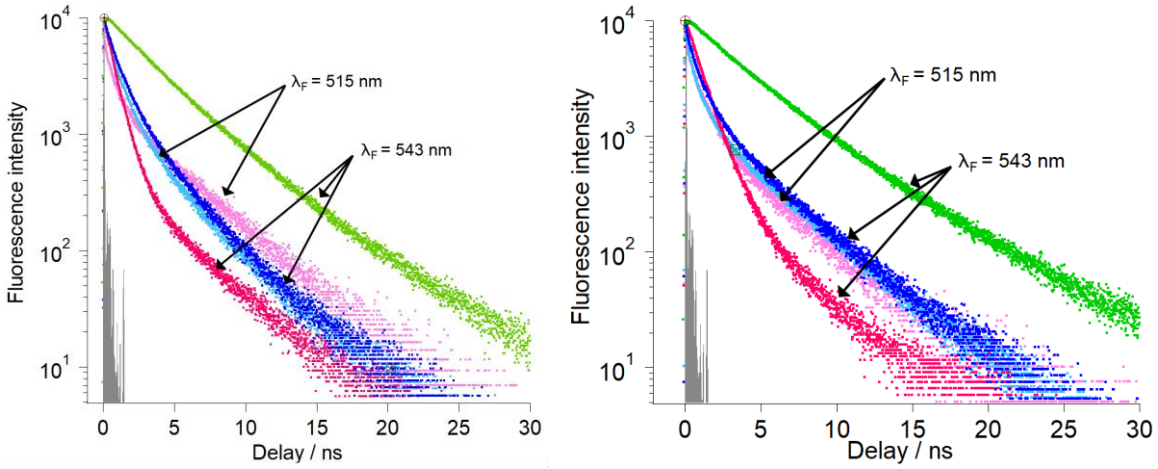

Figure S15. Fluorescence decays recorded in water at λ_F = 515 (lighter colors) and 543 nm (darker colors) (pH=7.8, λ_{ex} = 495 nm). Left: **$FNP1_{BOD}$** (green), **$FNP1_{FA}$** (blue) and **$FNP1_{BOD-FA}$** (pink). Right: **$FNP2_{BOD}$** (green), **$FNP2_{FA}$** (blue) and **$FNP2_{BOD-FA}$** (pink). Grey line is the instrument response function (IRF).

Multivariate curve resolution

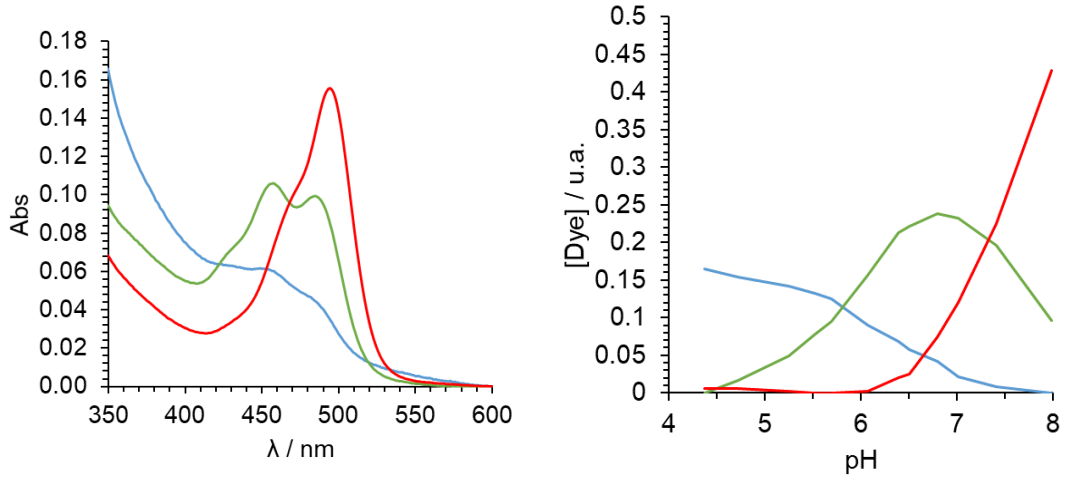

Figure S16. Left: spectral shape obtained from the multivariate curve resolution of the absorption spectra of **FNP1$_{FA}$** as a function of pH. The red spectrum corresponds to the one of the FA dianion, the green one to its anion and the blue to the neutral form. The increase in absorption at shorter wavelength is due to the scattering of light by the FNP. Right: distribution of the concentrations of the three species corresponding to the spectra on the left as a function of pH (same color code).

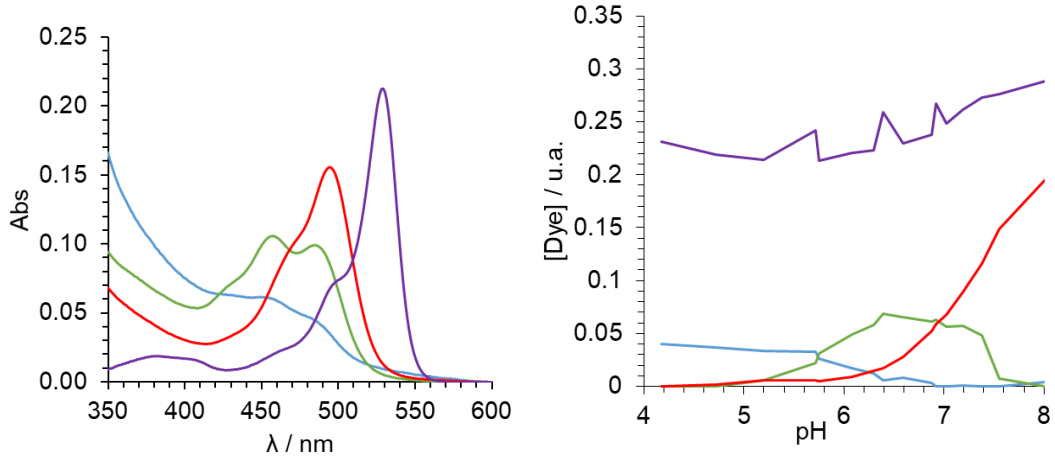

Figure S17. Left: spectral shape obtained from the multivariate curve resolution of the absorption spectra of **FNP1$_{BOD\text{-}FA}$** as a function of pH. The red spectrum corresponds to the one of the FA dianion, the green one to its anion and the blue to the neutral form and the purple one to the BODIPY. The increase in absorption at lower wavelength is due to the diffusion of light by the FNP. Right: distribution of the concentrations of the four species corresponding to the spectra on the left as a function of pH (same color code). The distribution for the FA components matches the one obtained with **FNP1$_{FA}$** while the contribution of the BODIPY shows a small variation.

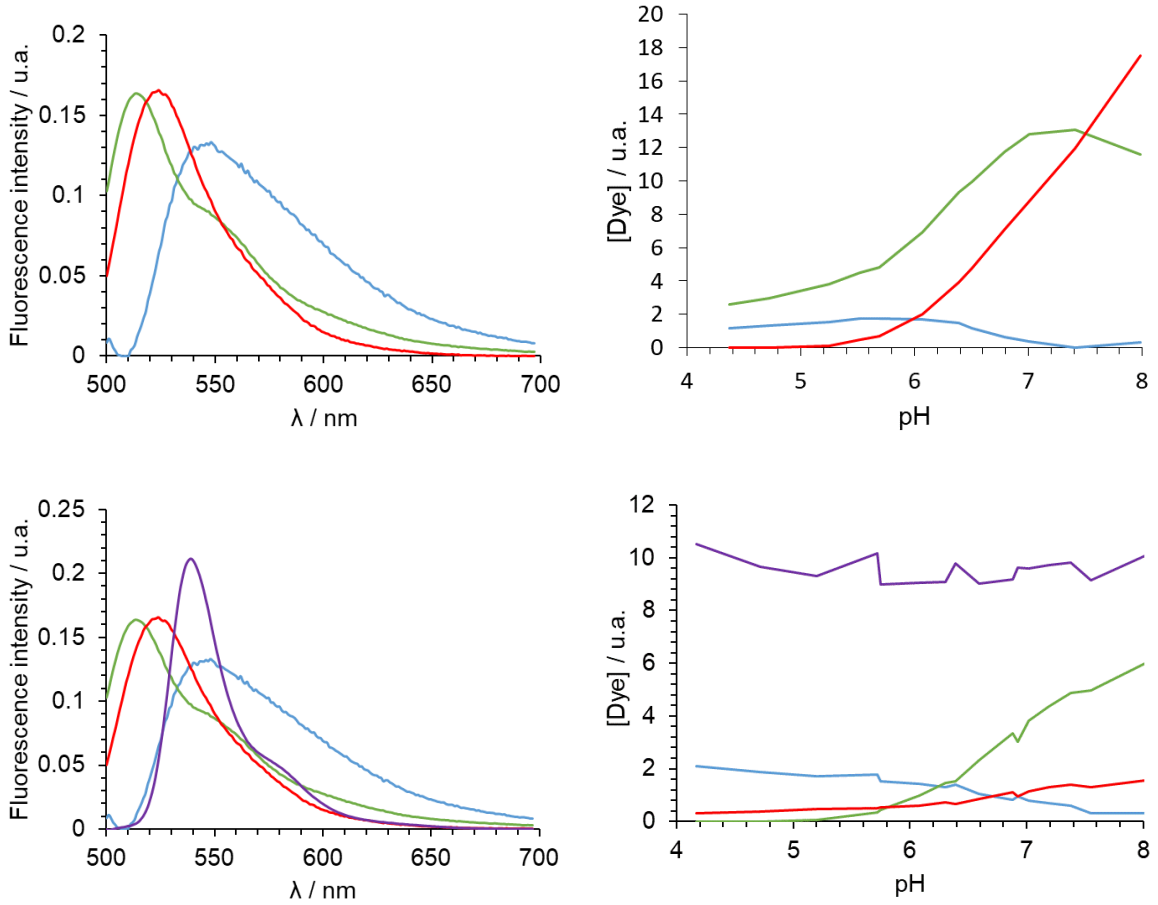

Figure S18. Top left: spectral shapes obtained from multivariate curve resolution of the emission spectra of **FNP1$_{FA}$** at different pH (from figure S9). The red spectrum matches the FA dianion, but the green and blue spectra do not correspond to known forms of the FA at different pH. Top right: distribution of the contributions of the three species corresponding to the spectra above as a function of pH (same color code). Bottom left: spectral shapes obtained from the principal component analysis of the emission spectra of **FNP1$_{BOD\text{-}FA}$** at different pH (from figure 2 left). The purple spectrum matches the BODIPY, the three other contributions are identical to the previous ones. Bottom right: distribution of the contributions of the four species corresponding to the spectra above as a function of pH (same color code). The contribution of the BODIPY shows small variation (5%) across the pH range studied.